Master's thesis

NTNU
Norwegian University of Science and Technology
Faculty of Natural Sciences
Department of Materials Science and Engineering

Magnus Høiberg Ødegaard

Modelling Grain Growth with the Phase Field Method

Master's thesis in Materials Science and Engineering
Supervisor: Professor Knut Marthinsen
June 2019

NTNU
Norwegian University of
Science and Technology

Magnus Høiberg Ødegaard

Modelling Grain Growth with the Phase Field Method

Master's thesis in Materials Science and Engineering
Supervisor: Professor Knut Marthinsen
June 2019

Norwegian University of Science and Technology
Faculty of Natural Sciences
Department of Materials Science and Engineering

NTNU
Norwegian University of
Science and Technology

Acknowledgements

I would like to sincerely thank Professor Knut Marthinsen for his help and guidance during this specialization project. Professor Marthinsen provided a foundation for this project both by providing metallurgical expertise as well as counsel with regards to the thesis work itself. Also, prior to the project, he lectured the subjects "Material and process modelling" and "Modelling phase transformations", relevant to this thesis.

I would also like to thank Dr. Tomas Manik, who assisted me in the upstart of this thesis, even though he was technically on paternity leave. He was also a co-supervisor in the project leading up to the start of this thesis.

Abstract

When a metal experiences grain growth, the grains, volumes of atoms with the same crystal lattice orientation, grow and absorb the smaller grains, resulting in a coarser structure with time. Understanding this process is integral to the field of physical metallurgy as well as advanced materials, as it can be observed to some degree in all high temperature material treatment.

Previous work describes methods for modelling grain growth with the phase field method, and a set of kinetic energy equations based on a free energy model. The phase field method has several advantages as compared to other, probabilistic models. The boundaries of grains are not tracked, and the boundaries themselves are diffuse, not sharp. This is achieved by assigning an order parameter η to all orientations available, and assigning a value representing the relative amount or alignment to this order for each node. The modelling procedure applies the kinetic energy equations by way of a spectral Fourier method, and all nodes in the grid are updated for each time step.

The initial grain structure is a randomly generated field of grains of random size and position, achieved with a Voronoi tessellation. The field edges are adjusted for periodic border conditions, matching the modelling procedure. This avoids pinning along the edges, which would greatly have affected the relatively small model grid, necessitating a larger grid and much slower modelling procedures. Grain size data are extracted at timed intervals.

The microstructural evolution is computed by the means of a spectral Fourier method, solving a semi implicit differential equation by the means of a spatial Fourier transform of the field variables. The data is compared to a similar Finite Difference scheme developed in an earlier project, as well as relevant thery.

Sammendrag

Modellering av kornvekst med fasefelt-metoden

Kornvekst i et metall innebærer at kornene, volumer med atomer med samme orientering av krystallstrukturen, vokser og absorberer mindre korn, hvilket resulterer i en mer grovkornet struktur. Å forstå denne prosessen er essensielt innenfor fysikalsk metallurgi så vel som avansert materialteknologi. Dette ettersom kornvekst kan observeres i alle former for varmebahndling av materialer.

Tidligere arbeider beskriver metoder for å modellere kornevekst med fasefelt-metoden, og et sett med kinetiske energiligninger basert på en fri-energi-modell. Fasefelt-metoden har flere fordeler sammenlignet med andre, probabilistiske metoder. Korngrensene blir ikke i seg selv etterfulgt, og grensene er diffuse, ikke skarpe. Dette er oppnådd ved å tilordne en ordensvariabel η til alle orienteringer i systemet. Variabelen blir gitt en verdi tilsvarende kornets relative tilhørighet til hvert enkelt korn, i alle korn. Modelleringsprosedyren bruker kinetiske ligninger med en spektral-Fourier-metode, og alle nodene oppdateres hvert tidssteg.

Kornstrukturen er i utganspunktet et tilfeldig generert område med korn med tilfeldig størrelse og posisjon. Dette gjøres ved hjelp av en Voronoi-tesselering. Kantene på området blir justert med hensyn til periodiske grensebetingelser, som er tilpasset modellerinsprosedyren. Med dette unngår man såkalt "pinning", at kornene fester seg langs kanten på området som modelleres, som kunne nødvendiggjort et større modellert område og tregere kjøretider. Informasjon om kornstørrelse blir hentet ut ved gitte tidsintervaller.

Microstrukturens utvikling beregnes ved hjelp av en spektral-Fourier-metode, som løser en semi-implisitt differensialligning ved hjelp av en romlig Fourier-transformasjon of fasefelt-variablene. Informasjonen sammenlignes med en lignende Endelig Differansemetode utviklet i et tidligere prosjekt, så vel som relevant teori.

Table of Contents

1 Introduction

When considering any material, microstructure is a factor affecting all properties, either structural or functional. The development of this with time potentially causing improvement, complications or failure. Computational modelling of microstructure development has proven to be a valuable tool, both saving hours of lab work, but also giving an insight into phenomena otherwise impossible to directly observe.

Grain growth occurs when recrystallization of the material is finished, and grain boundaries remain as the largest contribution to free energy in the system. The boundaries move, eliminating smaller grains, as the mean grain size increases. Phase field modelling is a relatively new development in computational physical metallurgy. Grain boundaries are described not with sharp borders, but with a set of field variables across the grain structure. The field variables represent the grain orientations of each point in the structure. Evolution of the grain structure is simulated with regards to free energy density, boundary migration kinetics, relaxation kinetics as well as the total free energy in an inhomogeneous system.

Significant developments in phase-field modelling where undertaken by Chen[1, 2] and Suwa[3] provide a useful basis and comparison data for the project. These in turn build on the work of Ginzburg and Landau[4], Cahn and Hillard [5], among many more.

This project aims to develop a phase field simulation of grain growth. The model should provide a realistic starting structure, with periodic borders to increase accuracy. The simulation will employ a spectral Fourier method for changes in the field variables. Data will be collected for grain sizes, and graphical representations of the grain structure at different instances will be generated.

This Master's thesis builds on previous project work the author conducted as part of a specialization project the Fall of 2018. That project developed a phase field model using the finite difference of modelling, and this will be used for comparison with this thesis.

2 Theory

In order to model the evolution of the grain structure it is apt to review basic grain-growth theory, as well as the principles of phase-field modelling. This theory is applied with kinetic and thermodynamic expressions for the behaviour of the material to obtain an evolution equation. Furthermore, for the Fourier Spectral method, a semi-implicit differential time discretization is applied and solved with the Fourier Transform.

2.1 Grain growth

The hard sphere model of physical metallurgy gives us an understanding of the metal atoms in volumes with uniform orientation. Between these grains lie grain boundaries. In the two-dimensional plane, low angle grain boundaries are characterized as lines of dislocations through the field of atoms with relatively low boundary energy, while high angle boundaries are either random fields of atoms with low density and high energies or special ordered boundaries with lower energy[6].

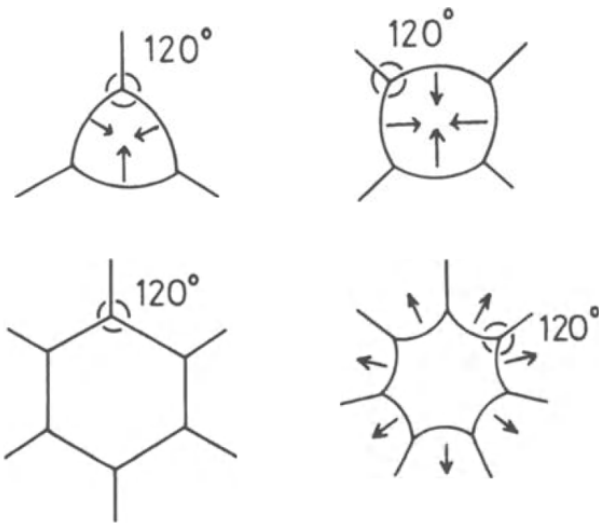

Figure 2.1: The effect of boundary curvature and triple point angles on grain growth direction[6].

.

The driving force of grain growth can be derived from the grain boundary being a defect in the crystal matrix, and the thermodynamic force towards reducing the area of the defect. The grains do not combine, the only mechanism of grain growth is the movement of grain boundaries. Characteristic features of grain growth can be observed geometrically. For a curved grain boundary, the driving force, and direction of grain migration, will be towards the centre of

curvature. Another rule applies to points where three grain boundaries meet, as shown in figure 2.1. Here the grain with the most acute angle will be diminished to the benefit of the other two. With this in mind, one can deduce that a hypothetical stable structure would consist of a field of identical even hexagons, where all angles between grain boundaries are 120 degrees[6]. Or put in terms of equilibrium between the boundary energies γ:

$$\frac{\gamma_{23}}{sin\theta_1} = \frac{\gamma_{13}}{sin\theta_2} = \frac{\gamma_{12}}{sin\theta_3} \tag{2.1}$$

The θ's are the angles in a three way junction. The atoms on the inside curve of a boundary experience a higher pressure, and will jump to the other side of the boundary to a position with less pressure. This has the effect that a curved boundary equates a difference in free energy that pushes atoms across the boundary. The change in free energy due to the boundary energy is

$$\Delta G = \frac{2\gamma V_m}{r} = \Delta\mu \tag{2.2}$$

Self-similarity

Figure 2.2 shows grain distribution plots for a couple of ideal hypothetical grain structures with time. The relative frequency distribution of grain sizes, from smaller to larger grains, has been shown to have a self-similar nature[7]. This means that the normalized (for mean size) grain distribution will have the same shape as time progresses. This will be an important effect for control of the accuracy of the model[8].

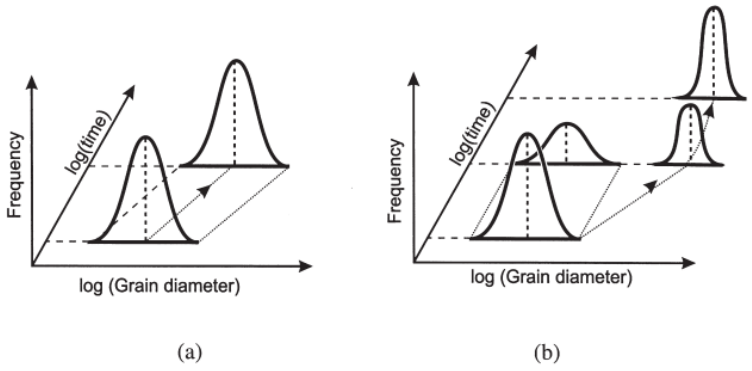

Figure 2.2: Self-similarity. Grain distribution plot for a) normal growth and b) abnormal growth[7].

.

2.2 Phase Field Modelling

Earlier regimes for modelling coarsening dynamics in materials have been largely based on defining the boundaries themselves as sharp[3]. Statistical models were developed for the movement of these borders through the material. This has the advantage of being simple to model without excessive use of computer resources. This however is not ideal for accurately modelling real systems.

A more recent development is the phase field model, taking a diffuse interface approach. Instead of defining hard borders, the matrix is discretized into points, each with defined grain orientation, and therefore grain affiliation. This way, the borders are implicitly defined by the values in each point,

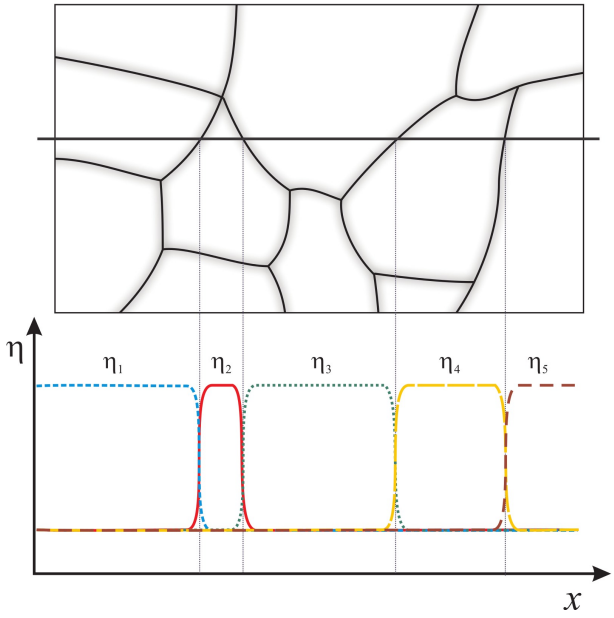

Figure 2.3: Illustration of phase field variables and their values through a cross-section of a grain structure.

In the phase field model, the grain affiliation of each point is defined by the field variables. These have a value for each position node in the system, and there can be any number of them, depending on necessity and resources. Figure 2.3 illustrates a grain structure with a field variable assigned to each grain. Along the x-axis from the left, the value of η_1 is one at first, then decreases close to a boundary, where η_2 increases to one and supplants η_1. The sum of the field variables in a single point is never higher than one, but can be lower than one in the grain boundary areas. Computation is applied to all variables in all nodes.

Phase field modelling has proven useful in biology, medicine, earth sciences as well as physical

modelling on a level above the atomistic.

2.3 Grain Boundary Migration Kinetics

The aforementioned difference in pressure and free energy on a grain boundary is also known as the Gibbs-Thomson effect, and can be written as

$$\Delta G = \frac{2\gamma V_m}{r} \tag{2.3}$$

Here the γ is the grain boundary energy, V_m is the molar volume, and r is the mean radius of curvature. We assume that the mean radius of curvature is proportional to the mean grain diameter of the system[6]. From this and the equation above we extrapolate that the mean grain growth driving force is proportional to $2\gamma/\overline{D}$:

$$\frac{d\overline{D}}{dt} = \alpha M \frac{2\gamma}{\overline{D}} \tag{2.4}$$

α is a constant for the order of unity, M is boundary mobility and $\overline{D}$ is the mean grain radius in the system. We say that $\overline{D} = D_0$ when $t = 0$, and integrate Equation 2.4 to get

$$\overline{D}^2 = \overline{D}_0^2 + Kt \tag{2.5}$$

where

$$K = 4\alpha M\gamma \tag{2.6}$$

Equation 2.5 can be rearranged to

$$\overline{R}^2 - \overline{R}_0^2 = kt \tag{2.7}$$

where $\overline{R}$ is the mean grain radius of the system, and $\overline{R}_0$ is the initial mean grain radius. Furthermore, as this project mainly operates in grain areas, the following relation is useful,

$$\overline{A} - \overline{A}_0 = kt \tag{2.8}$$

The field variables in the phase-field model are non-conserved, and consequently their evolution is linearly proportional to the derivative of free energy with respect to each variable. This means that a continuum Ginzburg-Landau equation describes

$$\frac{d\eta_i(r,t)}{dt} = -L_i \frac{\delta F}{\delta \eta_i(r,t)} \tag{2.9}$$

2.4 Total Free Energy

The work of Cahn-Hillard[5] in diffuse interface theory provides the total free energy of an inhomogeneous system as

$$F = \int \left[f(\eta_1(r), \eta_2(r), ..., \eta_p(r)) + \sum_{i=1}^{p} \eta_j \frac{\kappa_i}{2} \left(\nabla \eta_i(r)\right)^2 \right] d^3r \tag{2.10}$$

Here f is the local free energy density as a function of each local field variable. f should describe a density with equal minima at nodes with one $\eta = 1$ and the rest zero. That is, the minima describe the centre of a grain, where only one grain orientation is present. The second part of the expression is the gradient energy term for the boundaries, which equals zero at the minima, grain centres.

2.5 Free Energy Density

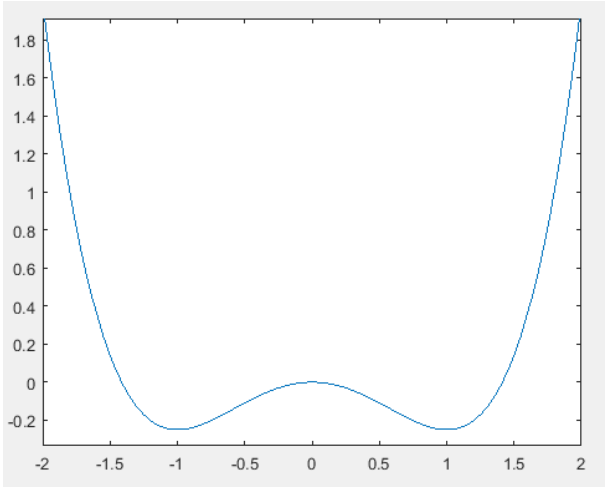

Figure 2.4: A plot of equation 2.12, with a double well shape.

The free energy function described above, simply needs to have minima where the field variable in question is 1. A function that fulfils this is as follows

$$f(\eta_1(r), \eta_2(r), ..., \eta_p(r)) = \sum_{i=1}^{p} \left(-\frac{\alpha}{2}\eta_i^2 + \frac{\beta}{4}\eta_i^4 \right) + \gamma \sum_{i=1}^{p} \sum_{j \neq 1}^{p} \eta_i^2 \eta_j^2 \tag{2.11}$$

The expression enclosed by the first summation, namely:

$$f = \frac{\alpha}{2}\eta_i^2 + \frac{\beta}{4}\eta_i^4 \tag{2.12}$$

describes the curve plotted in Figure 2.4. This function however, provides 2^p minima. To compensate, the latter summation is added. If γ is greater than $\beta/2$, then the total amount of minima is $2p$. This can be more clearly seen by re-writing equation 2.11:

$$f(\eta_1(r), \eta_2(r), ..., \eta_p(r)) = -\frac{\alpha}{2} \sum_{i=1}^{p} \eta_i^2 + \frac{\beta}{2} \left(\sum_{i=1}^{p} \eta_i^2 \right)^2 + \left(\gamma - \frac{\beta}{2} \right) \sum_{i=1}^{p} \sum_{j \neq 1}^{p} \eta_i^2 \eta_j^2 \tag{2.13}$$

2.6 Microstructure Evolution Equation

By substituting the total free energy F from equation 2.10 into the Ginzburg-Landau equation for the changes in field order parameters, equation 2.9, the following is obtained:

$$\frac{d\eta_i(r,t)}{dt} = -L_i \left(\frac{\delta f(\eta)}{\delta \eta_i(r,t)} - \kappa \nabla^2 \eta \right) \tag{2.14}$$

After the discussion in 2.5, function 2.11 can be substituted for f in this expression. In the end, after differentiating f, the following equation is obtained[9]:

$$\frac{d\eta_i}{dt} = -L_i \left(-\alpha\eta_i + \beta\eta_i^3 + 2\gamma\eta_i \sum_{j \neq i}^{p} \eta_j^2 - \kappa_i \nabla^2 \eta_i \right) \tag{2.15}$$

This is a microstructure evolution equation for the field variables in this phase-field model for grain growth. In the end, there are a number of variables in the expression,

- L_i: Kinetic coefficients, follows from the continuum equation 2.9. Standard value set to 1
- α, β and γ: Phenomenological parameters, these modifies the double well function 2.12 in equation 2.11 and controls the free energy aspect of the model. γ has been shown to have similar effect on grain growth as κ_i[3]. Standard values for all three set to 1.
- κ: Gradient energy coefficients, standard value set to 2.

The summation in this equation has a very logical, physical purpose. It sums the square of all field variables in the node except for the one in question for the change. This equates to zero in a node with only one field variable, and any other field variable will affect the change positively.

The Laplace operator ∇^2 in the last section governs the gradient energy, adding to the evolution of the field variable if the neighbouring nodes contain the field variable in question. This negatively affects the growth rate, which is appropriate; when a node is surrounded by identical nodes, it is located in the middle of a grain, and should not feel the energy gradient.

2.7 Semi-implicit Numerical Solution

In this project, the goal is to utilize the spectral Fourier method to solve a partial differential equation derived from the microstructure evolution equation. The spectral method is very robust compared to finite element methods, and tolerates coarser time discretization. This in turn allows for fewer time steps in the numerical solution scheme.

Equation 2.15 is fit for the finite difference method, but modification is necessary for the spectral method to be applicable. First of, the κ-expression is changed to apply semi-implicit time discretization:

$$\eta_{i,n+1} = \eta_{i,n} - \Delta t L_i \left(-\alpha \eta_{i,n} + \beta \eta_{i,n}^3 + 2\gamma \eta_{i,n} \sum_{j \neq i}^{p} \eta_{j,n}^2 - \kappa_i \nabla^2 \eta_{i,n+1} \right) \tag{2.16}$$

$\eta_{i,n}$ signifies the field variable for time t_n, what would normally be written as $\eta_i(t_n)$ and $\eta_{i,n+1}$ signifies $\eta_i(t_{n+1})$, a time-step forward. Then the spatial Fourier transform is applied:

$$\mathfrak{F}[\eta_{i,n+1}] = \mathfrak{F}[\eta_i] - \Delta t L_i \left(\mathfrak{F} \left[-\alpha \eta_i + \beta \eta_i^3 + 2\gamma \eta_i \sum_{j \neq i}^{p} \eta_j^2 \right] - \kappa_i k^2 \mathfrak{F} \eta_{i,n+1} \right) \tag{2.17}$$

Here the $\nabla^2 \eta_i$, the laplacian in real space, is transformed to the equivalent k^2, laplacian in Fourier space. The equation can be rearranged, sorting the time discretization:

$$\mathfrak{F}[\eta_{i,n+1}] + \Delta t L_i \kappa_i k^2 \mathfrak{F}[\eta_{i,n+1}] = \mathfrak{F}[\eta_i] - L_i \left(\mathfrak{F} \left[-\alpha \eta_i + \beta \eta_i^3 + 2\gamma \eta_i \sum_{j \neq i}^{p} \eta_j^2 \right] \right) \tag{2.18}$$

And finally, the equation used in the Spectral method is finished:

$$\mathfrak{F}[\eta_{i,n+1}] = \frac{\mathfrak{F}[\eta_{i,n}] - \Delta L_i \mathfrak{F}[-\alpha\eta_i + \beta\eta_i^3 + \gamma\eta_i \sum_{j\neq i}^{p} \eta_j^2]}{1 + \Delta t L_i \kappa_i k^2} \tag{2.19}$$

After the above is computed, a backwards Fourier transform is applied to the Fourier image:

$$\eta_{i,n+1} = \mathfrak{F}^{-1}[\mathfrak{F}[\eta_{i,n+1}]] \tag{2.20}$$

The result is a solution to the evolution equation that can be used in the spectral Fourier method.

3 Method

The project took the form of a program in the language C++, generating a randomized field of grains with random size and positions. The mathematical modelling itself is executed with a spectral Fourier method, with a finite difference method for comparisons. The result is graphics illustrating the grains themselves, as well as numerical data on the grain growth of the system modelled.

3.1 Grid structure

The Mesoscale Microstructure Simulation Project (MMSP) is an online repository containing tailored classes and class functions in the C++ programming language[10]. This resource simplifies a lot of the operations in this project, as they need special functions for accessing the data structure containing the phase field variables.

The main class in use is the GRID class. This data class consists of an array of predetermined size, in this application 256 by 256 nodes. Each node contains a vector with the number of field variables needed for the application. In this programme each field variable in the vector represents a possible orientation of the crystal grid. They can have a value between zero and one, representing the nodes affinity towards each possible orientation. In the middle of a grain, a single field has the value one, while the others have the value zero. In the diffuse grain boundaries, two or more fields have a value smaller than zero, but with a sum lower than one. This corresponds with the theory illustrated in Figure 2.3 on page 4.

```
double **etas;
etas = (double**)calloc(Netas, sizeof(double*));
for (int i = 0; i < Netas; ++i) {
        etas[i] = (double *)calloc(Nodes, sizeof(double));
}
```

The Fourier library used for the spectral variant of the simulation, however, was not compatible with this class. To run a Fast Fourier Transform, the data had to be put in separate arrays for each field variable. Each of these arrays would represent a full grid of nodes for one single field variable. For storing data between data collection sequences, these arrays were combined into a nested array for storage in a cache file. For 36 field variables in a grid of 256 by 256 nodes, this nested array would contain over 2.3 million doubles. An array of this size is to large for the stack in the memory hardware for many machines, so the class is allocated to the heap by using the calloc-command in C++. This necessitates handling of pointers, as well as manually

handling and freeing memory. The code for the allocation of this nested array can be seen above this paragraph.

The MMSP GRID-class was however used for visualization and comparisons between the Finite Difference and Fourier Spectral methods. This is discussed further in section 3.4.

3.2 Initial grain structure

A notable difference between the procedure developed in this project and the techniques of Chen[1, 2] and Suwa[3] is how the initial grain structure is generated. The aforementioned reports initializes the programme by assigning the given number of field order variables randomly to every single node. This gives a somewhat liquid-like and certainly random initial structure, but this model has no way to account for liquid kinetics. There is also the problem of grains with the same orientation field variable "finding" each other and merging as the grains grow. In this project, it was deemed appropriate to generate a field of grains somewhat similar to an actual solidified metal.

Voronoi tessellation

A Voronoi Tessellation is a method for dividing an area into randomly placed smaller areas of random size and shape. It is named after Georgy Voronoi. The tessellation implemented in this project initially distributes a set of seed points randomly across the area. Each node in the system then measures the distance to all seed points, and finds the closest one. The orientation field variable for the node corresponding to the chosen seed point is set to one, while all other are set to zero. The result is structure closely resembling a natural grain structure in a pure unalloyed metal. Each orientation field variable is assigned to exactly one grain in the structure. The grain boundaries are sharp before the simulation starts, but immediately become diffuse as the programme commences.

Periodic border conditions

An issue that arises when the basic tessellation is finished, is the matter of the borders of the modelling field, illustrated in Figure 3.1a. At these edges the grains stretch, as there are no grains outside the field for the Voronoi procedure to consider. In effect there is a pinning around the edge, an unwanted factor when modelling pure grain growth. This limits the accuracy of the model closer to the edge, an effect that becomes more prevalent as the grains grow and become more affected by the border grains.

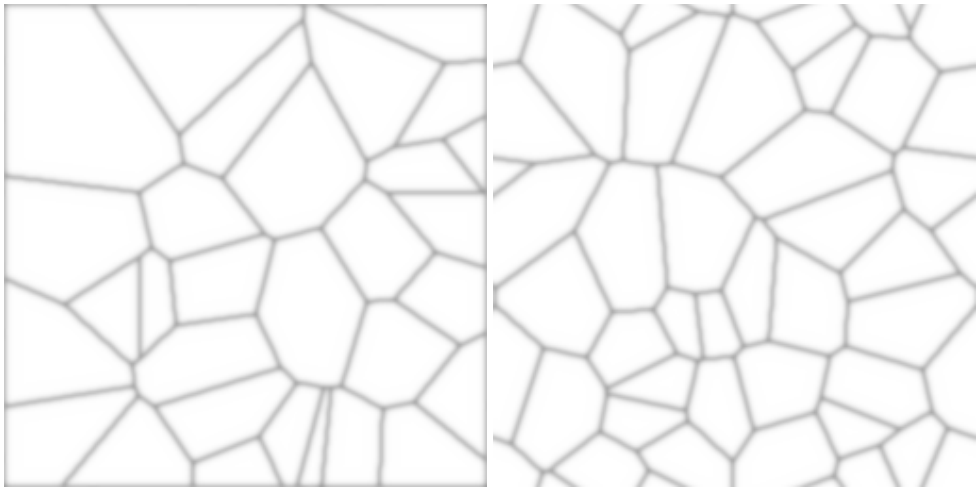

(a) Voronoi Tessellation without periodic border conditions.

(b) Voronoi Tessellation with periodic border conditions.

Figure 3.1: Comparison of Voronoi Tessellation with and without periodic border conditions. Other parameters are identical, but the placement of the grain seeds are random. Notice the shape of the grains close to the edges.

The solution in this project was to initially generate a much larger modelling area. The initial grid is a three-by-three repetition of the intended field, an area nine times as large. Each of the eight identical copied fields have the same seed points as the original, relative to the copied field itself, see Figure 3.2. When the tessellation is finished, the program separates the field in the centre from these nine, and continues with the procedure. This means that a node at the edge of the intended modelling area will detect a seed point outside of the field, placed as if the field repeats periodically and the closest point is on the other side of the field. Fields at the edges will not expand towards the edges that pin them, but enclose an area defined by a seed point outside the frame.

For this implementation to work, another issue has to be addressed; the program has to know that two grains on opposite edges of the field has the same crystal orientation. In the model, this means that the same η on both sides need to have the value 1 for a pure grain. This is done by comparing all nodes along the top edge of the field with the bottom, and the right with the left. The programme then checks all nodes in the field if they belong to these grains, and sets their field variables correspondingly. This is a time consuming process, but is only done once for each grain structure.

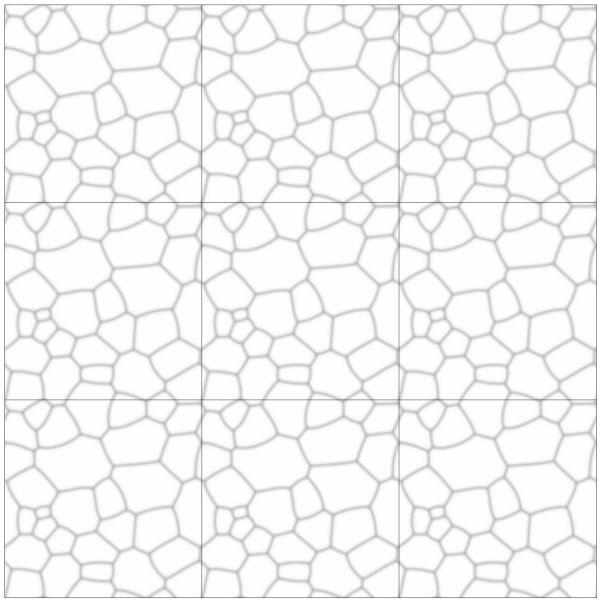

Figure 3.2: A three-by-three grid, repeating the initial Voronoi Tessellation.

3.3 Numerical Implementation

With the initial grain structure generated, the next step is the numerical procedure itself. This project utilizes both a finite difference method as well as a spectral Fourier method for modelling the grain growth. This builds on earlier work, and allows for useful comparisons[11].

Finite Difference Method

The programme employs equation 3.1, see page 7 in Theory for details, in a finite difference scheme. For each node in the MMSP-grid class, the vector of field variables is evaluated, and change calculated for each variable. The iterator i indicates the current field variable, and j indicates all other field variables in the node.

$$\frac{d\eta_i}{dt} = -L_i \left(-\alpha\eta_i + \beta\eta_i^3 + 2\gamma\eta_i \sum_{j\neq i}^{p} \eta_j^2 - \kappa_i \nabla^2 \eta_i \right) \tag{3.1}$$

The laplacian in the rightmost part of the expression governs the gradient energy, adding to the evolution of the field variable if the neighbouring nodes contain the field variable in question. This laplacian is calculated with the code seen below, for a single node and a single eta.

```
for (int i=0; i<dim; i++) {
    s[i] += 1;
    const T& yh = GRID(s);
    s[i] -= 2;
    const T& yl = GRID(s);
    s[i] += 1;

    laplacian += (yh - 2.0 * y + yl);
}
return laplacian;
```

Semi-implicit Fourier Spectral Method

The improved scheme for simulating the microstructure evolution utilizes a fast Fourier transform to solve a semi-implicit differential version of the microstructural evolution equation. Since this method computes on a Fourier Transform Spectre of the field, it is called the Spectral Method.

The Spectral Method for modelling the grain evolution required Fourier transforms of each phase field grid, which there was 36 of for most of the procedures. This was achieved by employing the free FFTW library, developed at MIT[12]. As can be seen in equation 3.2 and 3.3, the procedure necessitates running three separate transforms, one for each of the Fourier transforms in the denominator of equation 3.2, and one backwards transform for equation 3.3, to resolve the full solution.

$$\mathfrak{F}[\eta_{i,n+1}] = \frac{\mathfrak{F}[\eta_{i,n}] - \Delta L_i \mathfrak{F}[-\alpha\eta_i + \beta\eta_i^3 + \gamma\eta_i \sum_{j\neq i}^{p} \eta_j^2]}{1 + \Delta t L_i \kappa_i k^2} \tag{3.2}$$

$$\eta_{i,n+1} = \mathfrak{F}^{-1}[\mathfrak{F}[\eta_{i,n+1}]] \tag{3.3}$$

In equation 3.2, the k^2 in the numerator, similarly to the ∇^2 for the finite difference method, is the laplacian of the field variables. The important difference in this case, is the fact that this computation is done in Fourier space, and thus the laplacian values need to be in the same space. Since this field of laplacians only is dependent on the field dimensions in Fourier space, and not the values in the nodes themselves, they could be calculated separately. To save computation time, this was done only once per program call. The code for generating this laplacian can be seen below.

```
for (int k = 0; k < Nx21; k++) {
    fk1 = (k)*delkx;
    kx[k] = fk1;
    kx[Nx2 - k + 1] = -fk1;
}

for (int k = 0; k < xdim; k++) {
    for (int l = 0; l < xdim; l++) {
        k2[k + l*xdim] = (pow(kx[k], 2) + pow(kx[l], 2));
    }
}
```

Note that, unless otherwise specified, the standard values for the parameters were set to 1 for all except κ which was set to 2.

3.4 Data collection

The procedure does not save grid structures for the whole system at every time-step, as this would quickly fill computer memory. The initial program call, rather, has the user provide the total number of time steps as well as the intermediate data collection interval. Large grain structure grid files can reach several megabytes in size, and for long simulations, this could lead to gigabytes of data. Generally 20 time intervals where employed in the analysis below.

The most important data value for comparison with other projects is the grain fraction of the grains in the system, and the mean grain fraction of the whole system. This is collected in a pure text file, which can be read by any suitable analytical tool. Matlab was used in this project.

FFT-array

In order to use the FFT functions in the FFTW3 library, the data was put in a nested array structure, as described in section 3.1. To save computation time, this structure was saved outside the program between time steps, instead of the GRID-class. For every data collection step, however, the data is also saved as a GRID-class, for comparison to previous data. The result of this is a minuscule increase in processing time, but the benefit of advanced visualization outweighs this.

Self-similarity and other comparisons

In order to make a ascertain the self-similarity of the grain distributions, it is necessary to construct a grain size distribution plot. A single run of the programme, however, starts with 36 grains, and this number is reduced. This is not a sufficient number of grains to retrieve a statistically significant data set. The solution to this was to run several parallels with identical parameters, but random starting structures. Identical starting structures would result in duplicate data.

For the comparison between the spectral method and finite difference method, as well as the expected nature of the grains size distribution, a script for bulk processing was utilized. Ten parallels were run for each method, a number balancing the need for data, processing power and available time. It should be noted that since the spectral method used more time per operation, but with a high tolerance for time discretization, the latter was set to $dt = 1$, as compared with $dt = 0.1$ for the finite difference program. A dt of 0.1 is quite close to the breaking point for this method, while the spectral method managed $dt = 1$ easily. Thus slower processing time is accounted for in the final result.

4 Results

Figure 4.1 shows the evolution of the grain structure from a recently Tessellated structure in the beginning, to larger grains eating the smaller ones in the fourth and fifth picture. The white areas represent pure grains with a single grain orientation, while the grey lines are the diffuse borders, where the field variables have a value below one. The time between the images is not linear, rather, the images have been picked to best show the relative growth and shrinking of the grains. Picture 3, 4 and 5 shows a relatively stable and even hexagon in the top right, demonstrating the effect discussed on page 2 and shown in figure 2.1.

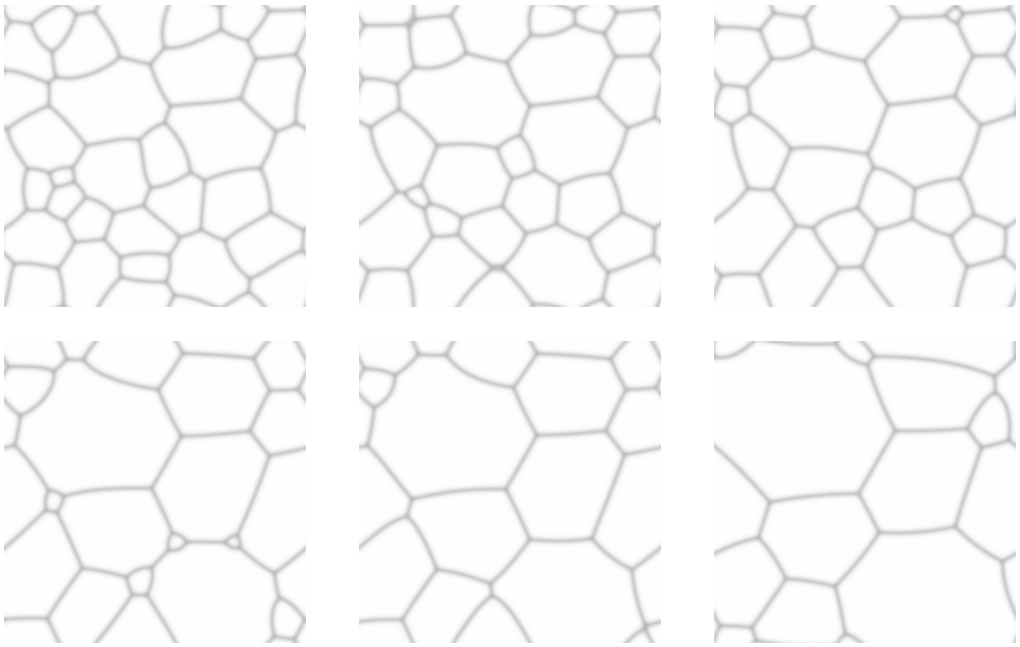

Figure 4.1: Visualization of the grain evolution in the model.

It is important to note that the grain growth curve from a single run is neither linear nor smooth, but has rather stepped form, as can be seen below in Figure 4.3. This is due to the mean grain size being dependent on the total number of grains, an integer that changes abruptly whenever a single grain size reaches zero, see equation 4.1. To account for this in collecting data, several parallels or consecutive runs have to be performed. In this project, most data was collected from means over 10 runs. Figure 4.5 shows the mean grain size over 10 different runs, along with the mean of these runs. With more parallels the mean value of these means becomes smoother and more linear.

$$\overline{A} = \frac{\sum A_{\eta,i}}{N} \tag{4.1}$$

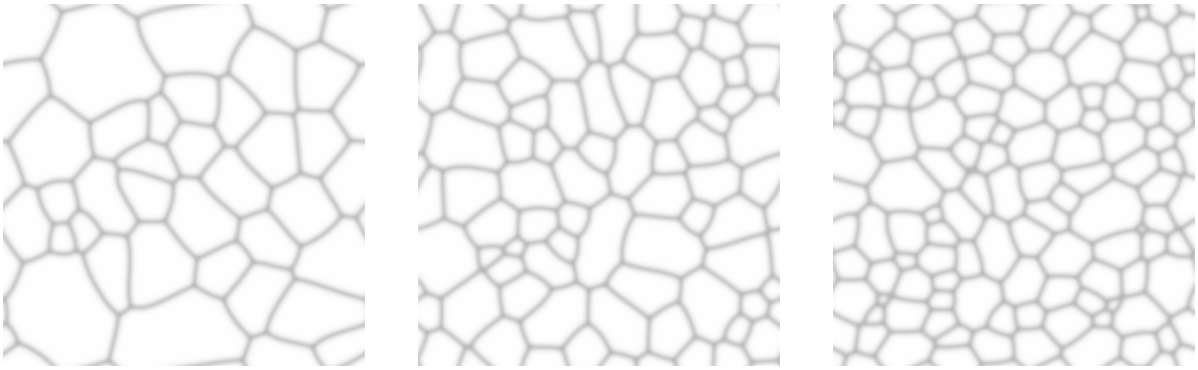

(a) 36 grains **(b)** 72 grains **(c)** 130 grains

Figure 4.2: Starting structure with different grain numbers/ field variables.

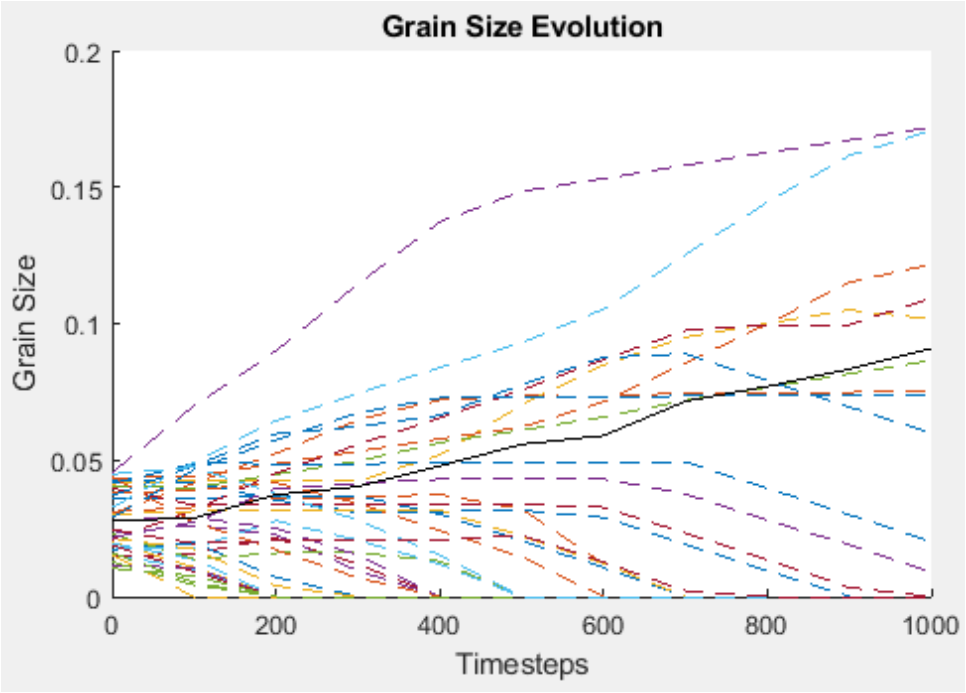

Figure 4.3: Evolution of grain sizes for a single structure. Dotted lines are individual grains/field variables, and the solid line is the mean grain size.

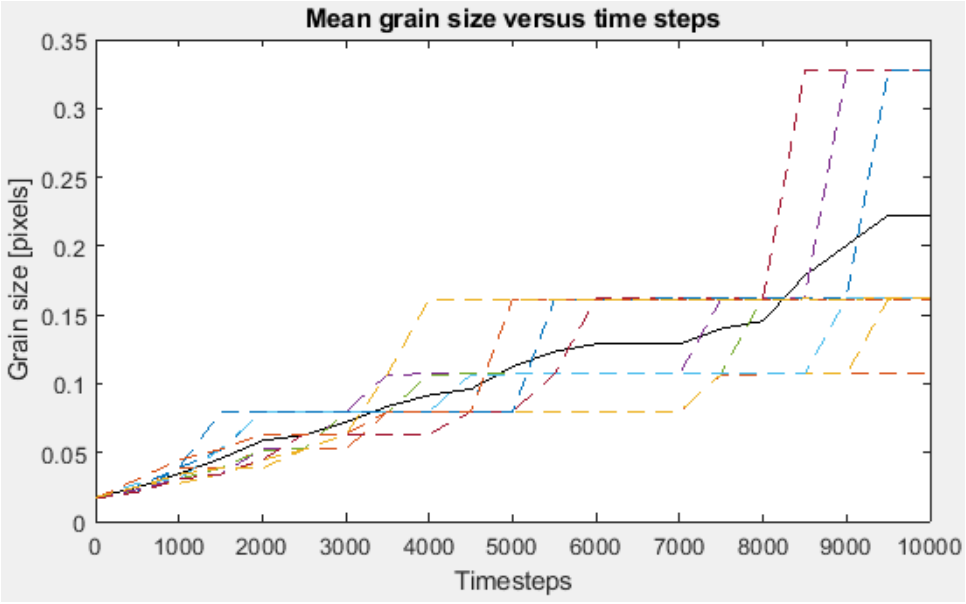

Figure 4.4: 18 Grains. Mean grain size evolutions of 10 different grain structures. All parameters are identical, but the initial structure is randomized. The dotted lines are individual mean grain sizes and the solid line is the mean.

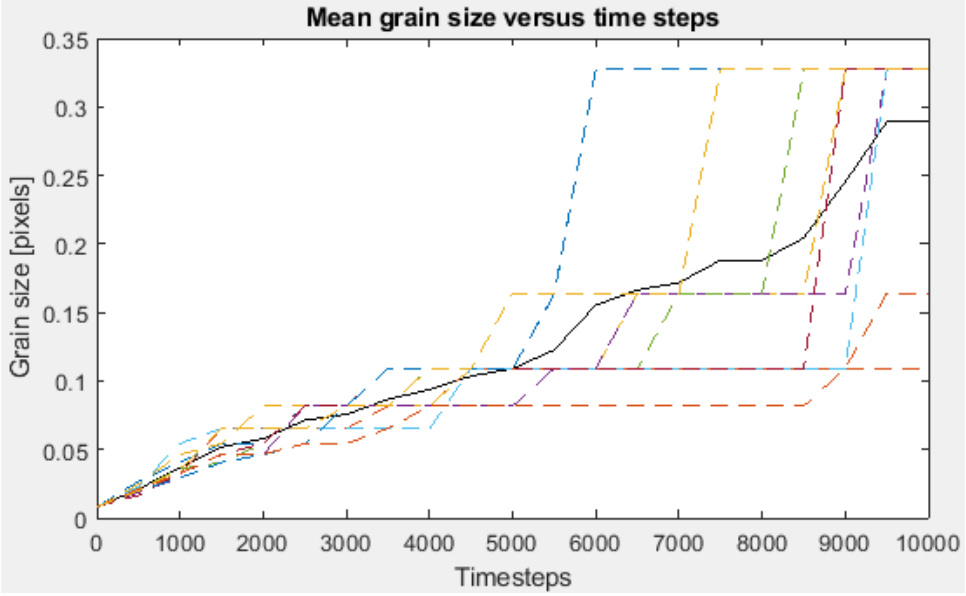

Figure 4.5: 36 Grains. Mean grain size evolutions of 10 different grain structures. All parameters are identical, but the initial structure is randomized. The dotted lines are individual mean grain sizes and the solid line is the mean.

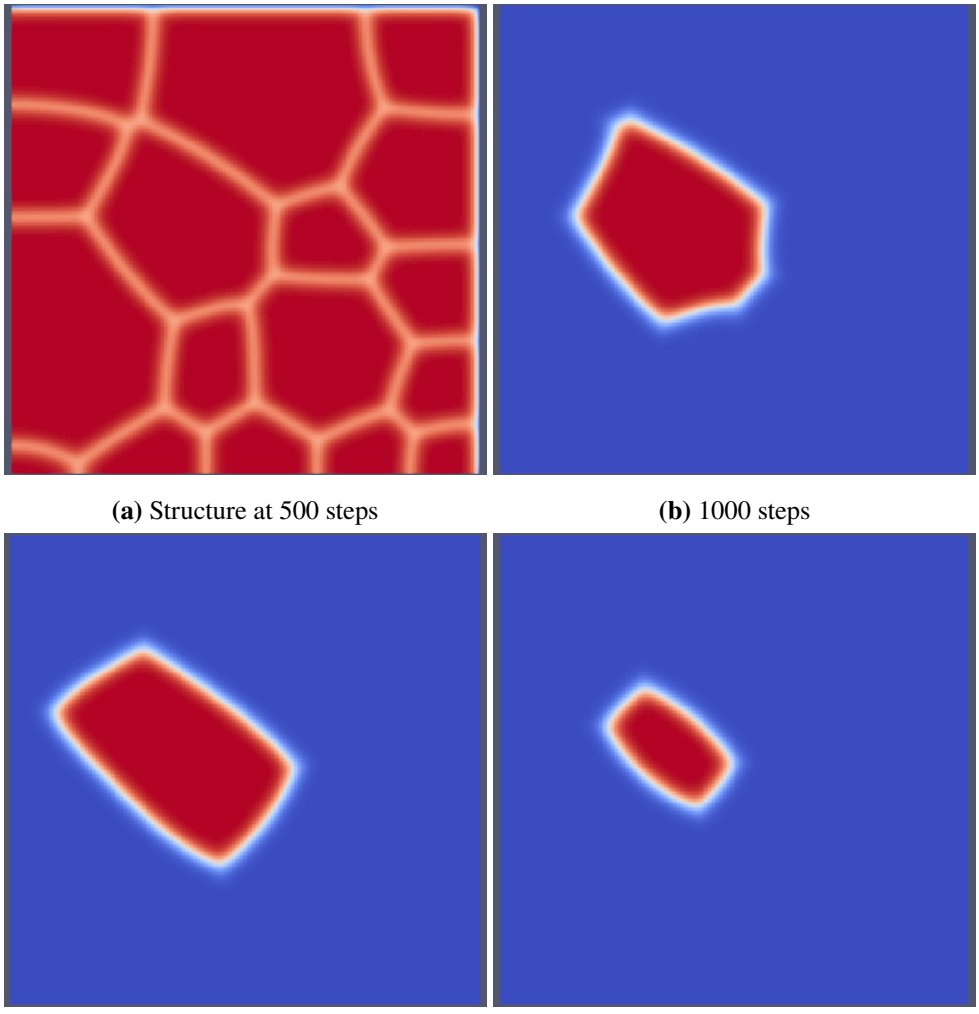

(a) Structure at 500 steps **(b)** 1000 steps

(c) 1500 steps **(d)** 2000 steps

Figure 4.6: Evolution of a single grain, as well as the initial surrounding grain structure. Spectral method, dt = 1. This also shows how the structure is analysed using software, separating the data for each grain.

Figure 4.6 shows evolution of a single grain, chosen from an initial field of grains.

4.1 Effect of Parameters

The Microstructure Evolution Equation for the Spectral Method, Equation 3.2, has a number of parameters, as discussed in Section 2.6. This section presents the result of varying three of them, γ, κ and the kinetic coefficient, L.

$$\mathfrak{F}[\eta_{i,n+1}] = \frac{\mathfrak{F}[\eta_{i,n}] - \Delta L_i \mathfrak{F}[-\alpha\eta_i + \beta\eta_i^3 + \gamma\eta_i \sum_{j\neq i}^{p} \eta_j^2]}{1 + \Delta t L_i \kappa_i k^2} \tag{4.2}$$

Equation 4.2 above, is provided for reference.

L - Kinetic coefficient

Figures 4.7 and 4.8 show the result of varying the parameter L between 0.5 and 3.

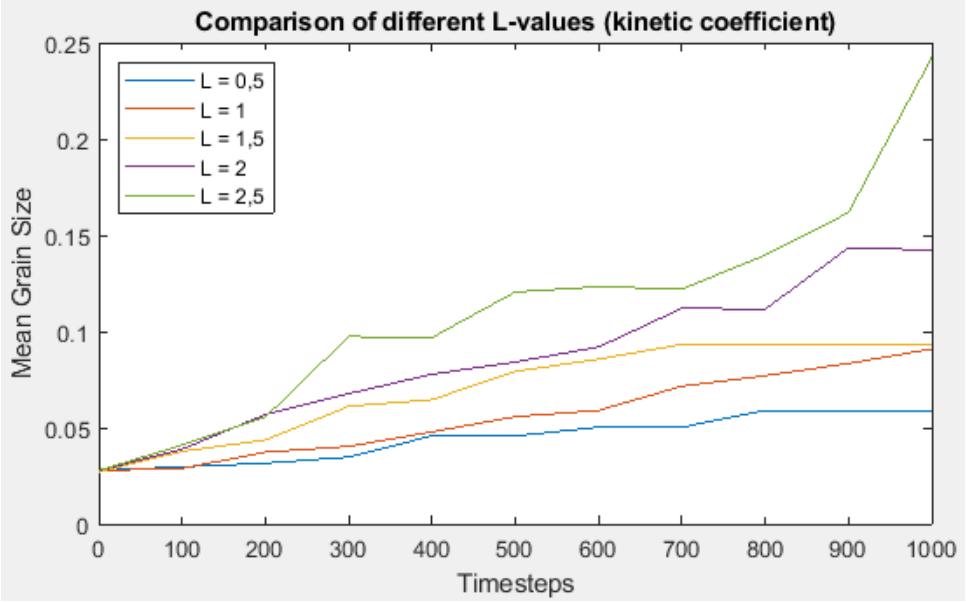

Figure 4.7: Average grain size plotted for five different -values.

.

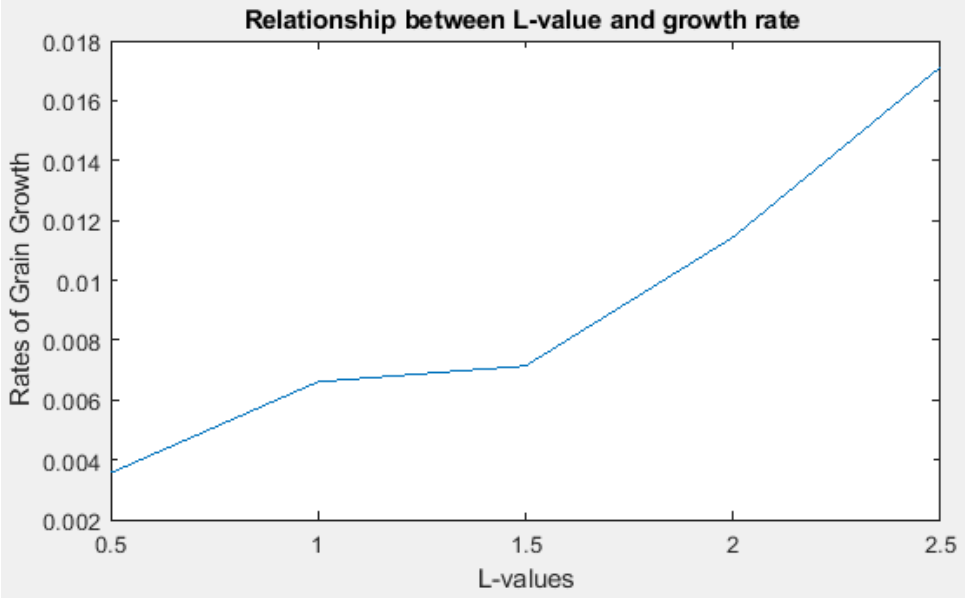

Figure 4.8: Grain growth plotted for increasing L-value.

.

κ - kappa

Figures 4.9 and 4.10 show the result of varying the parameter κ between 0.5 and 2.5.

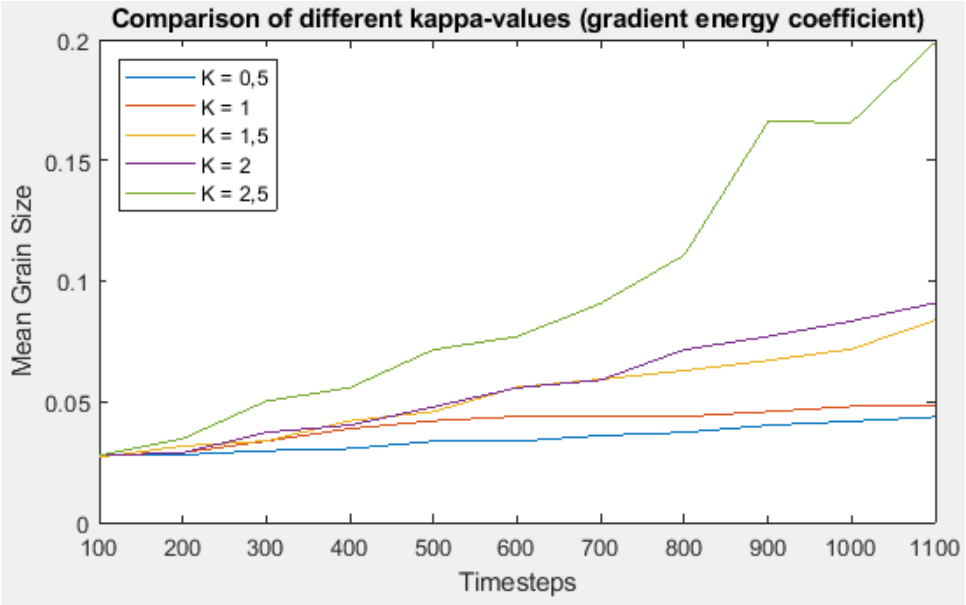

Figure 4.9: Average grain size plotted for five different κ-values.

.

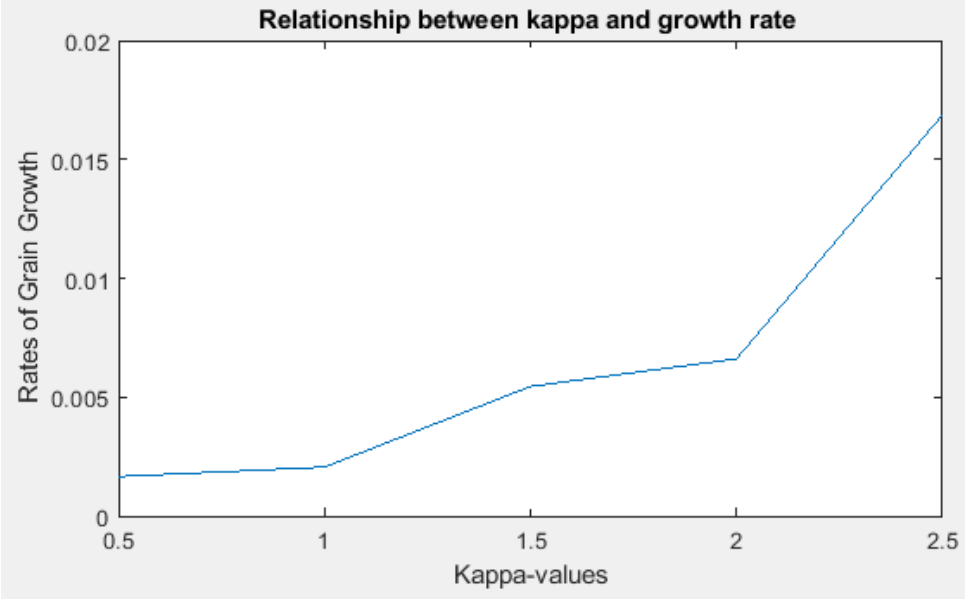

Figure 4.10: Grain growth plotted for increasing κ-value.

γ - gamma

Figures 4.11 and 4.12 show the result of varying the parameter γ between 0.5 and 3.

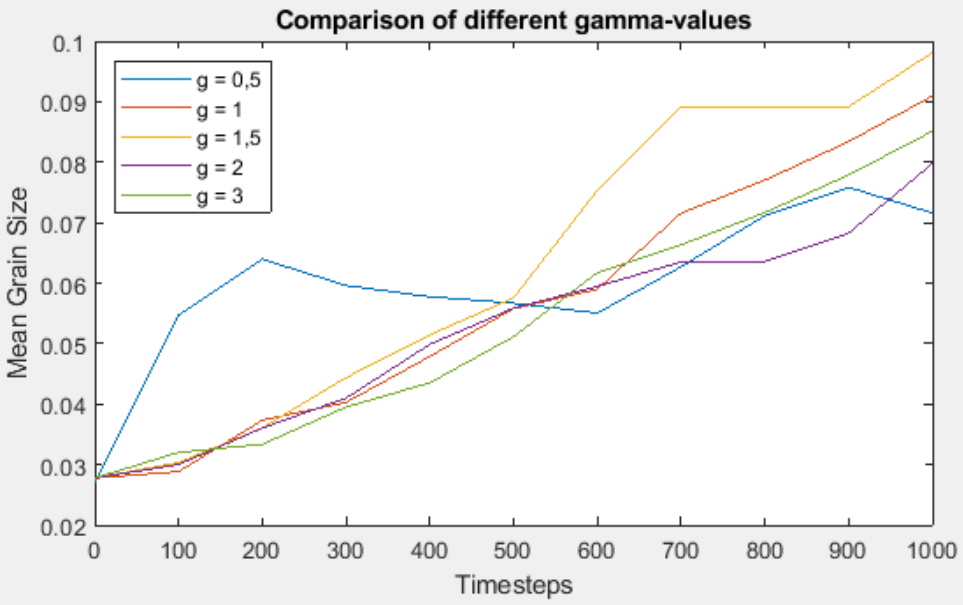

Figure 4.11: Average grain size plotted for five different γ-values.

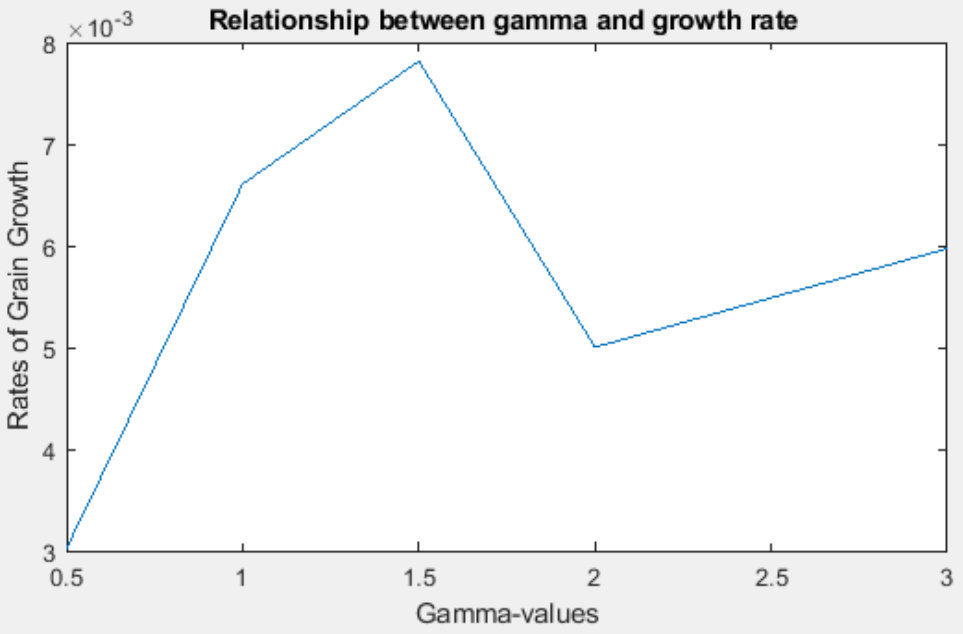

Figure 4.12: Grain growth plotted for increasing γ-values.

5 Discussion

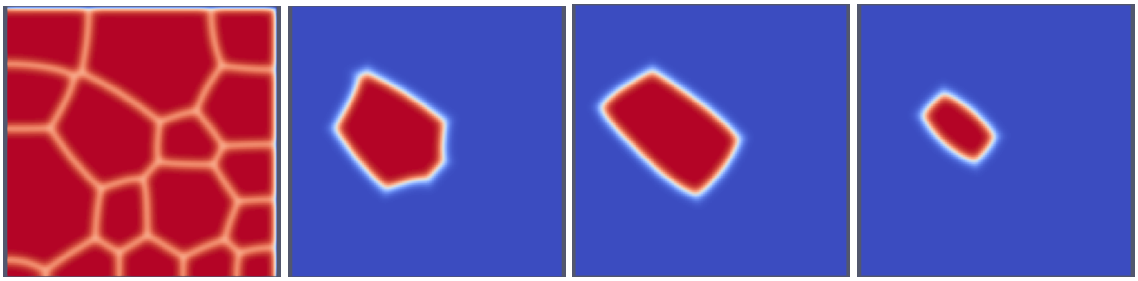

(a) Structure at 500 steps **(b)** 1000 steps **(c)** 1500 steps **(d)** 2000 steps

Figure 5.1: Evolution of a single grain, as well as the initial surrounding grain structure. Spectral method, dt = 1. This also shows how the structure is analysed using software, separating the data for each grain.

Figures 5.1 shows the development of one grain, separated from the rest of it's system. Between Subfigures 5.1b and 5.1c the grain seems to grow. This appears to be due to neighbouring, smaller grains diminishing, and this grain gaining size to their detriment. After this, however, the grain is no longer a large grain compared to it's neighbours, and it starts shrinking. The fifth picture in this sequence was not included, as it was simply a field of blue, the grain not existing any more.

This is in accordance with the grain growth theory in section 2.1. If we consider the curvature of the sides of the grain instead, we see that the expansion happens on the three sides that are clearly curving towards the grain itself. Here the driving force of grain growth pulls the boundary towards the grains with higher free energy.

Below, Figure 5.2 shows a full set of grain size plots, one dotted line for each single grain in the system. As anticipated, a number of grains are reduced immediately, letting others grow. Some grow in size before shrinking, like the grain in Figure 5.1. The mean, as explained in the Results section, is not linear, and Figure 5.3 shows the mean curve of 4 parallels.

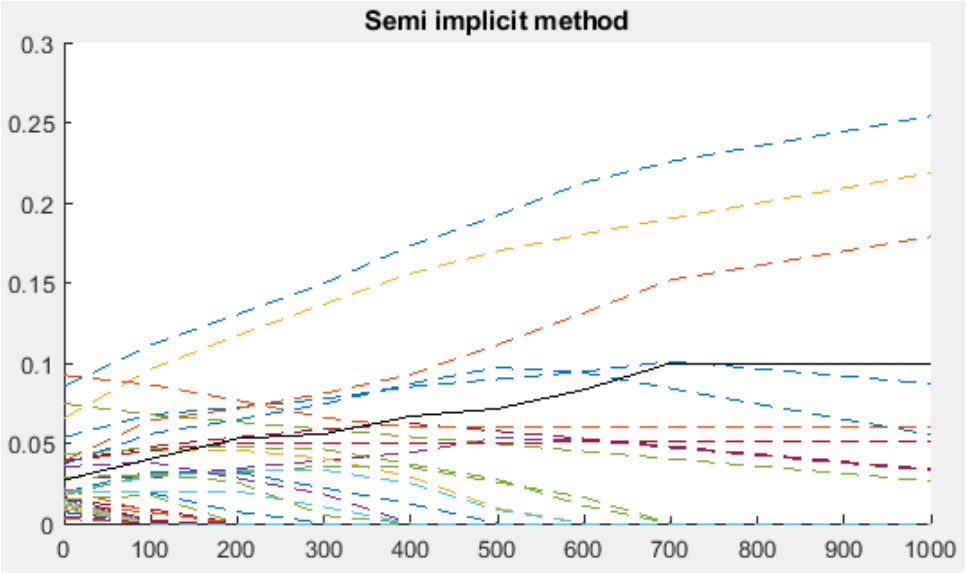

Figure 5.2: 1000 steps of evolution for a structure with 36 initial grains.

.

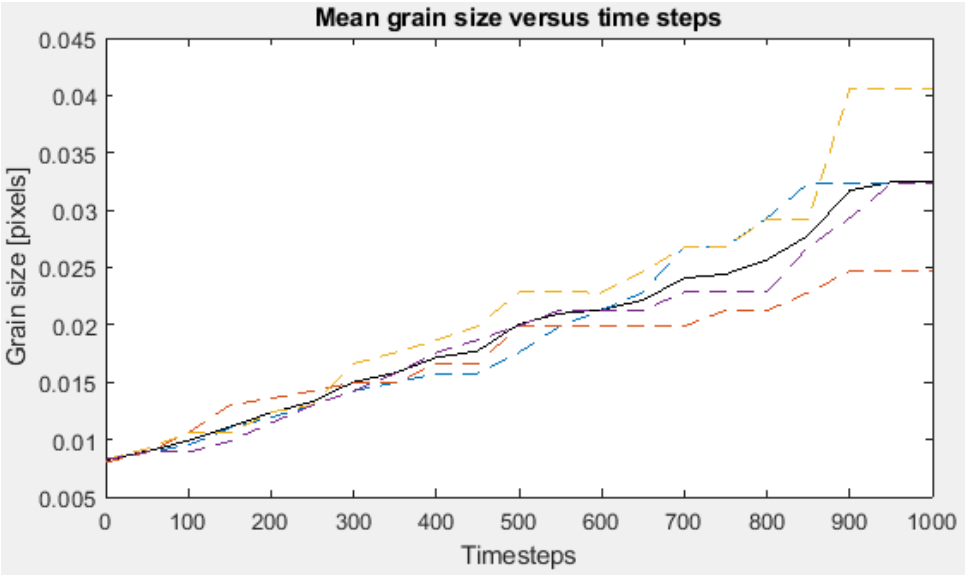

Figure 5.3: 1000 steps of evolution for a structure with 36 initial grains.

.

5.1 Parameters

L - Kinetic coefficient

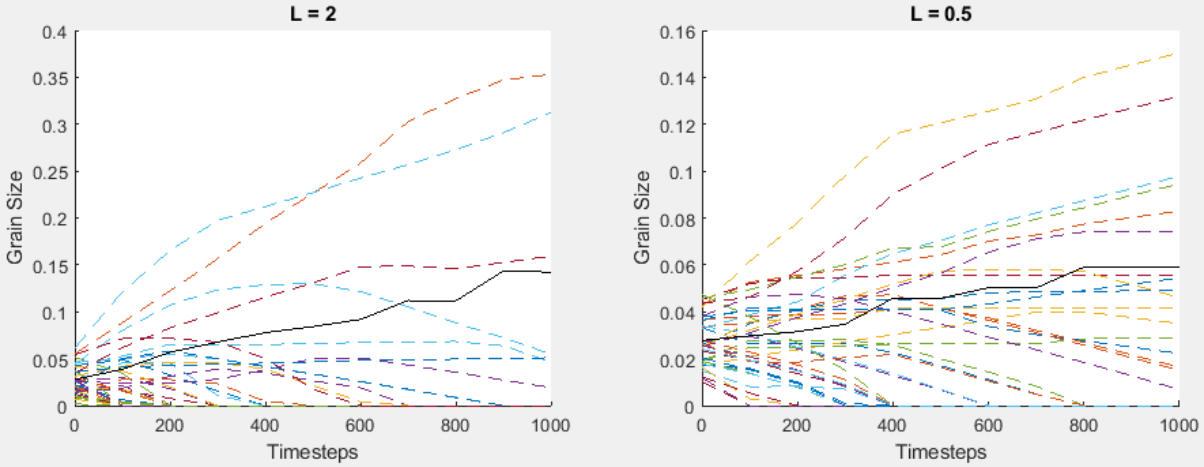

Figure 5.4: Comparison of L-values. Plotted are the size of each grain with dotted lines, and the average grain size with a solid line.

.

Below is a comparison of the growth curves for all grains for two different values of the kinetic coefficient, L. The plots are quite similar, the main difference being many grains diminishing fast with the higher of the two values. Figures 4.7 and 4.8 show that the change in growth rate follows a curve that might be exponential or cubic. From the highest value for L, 3, seems to also tend towards being exponential, but this might be coincidental.

κ - kappa

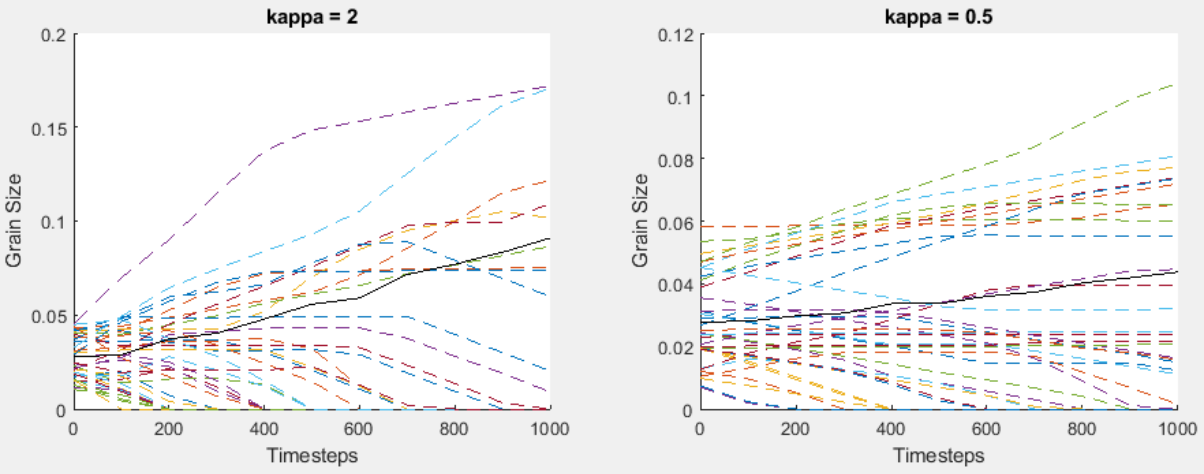

Figure 5.5: Comparison of κ-values. Plotted are the size of each grain with dotted lines, and the average grain size with a solid line.

.

Overall, κ seems to have a very similar effect on the growth rate as L. For lower values, the growth curves in 4.9 are some of the most even produced in this project. κ is an energy gradient coefficient and in Equation 4.2, κ is a factor in front of the k^4 laplacian of the field. Higher values significantly increases growth rate, which also means that grains shrink faster. The plot comparing growth rates 4.10 has a shape that looks even more exponential than that of L.

Parameters\Values	0.5	1	1.5	2
L	$3.6 * 10^{-}3$	$6.6 * 10^{-}3$	$7.1 * 10^{-}3$	$11.4 * 10^{-}3$
γ	$3 * 10^{-}3$	$6.6 * 10^{-}3$	$7.8 * 10^{-}3$	$5 * 10^{-}3$
κ	$1.7 * 10^{-}3$	$2.1 * 10^{-}3$	$5.4 * 10^{-}3$	$6.6 * 10^{-}3$

Table 5.1: Comparison table of parameters and their resulting rates of mean grain growth.

γ-gamma

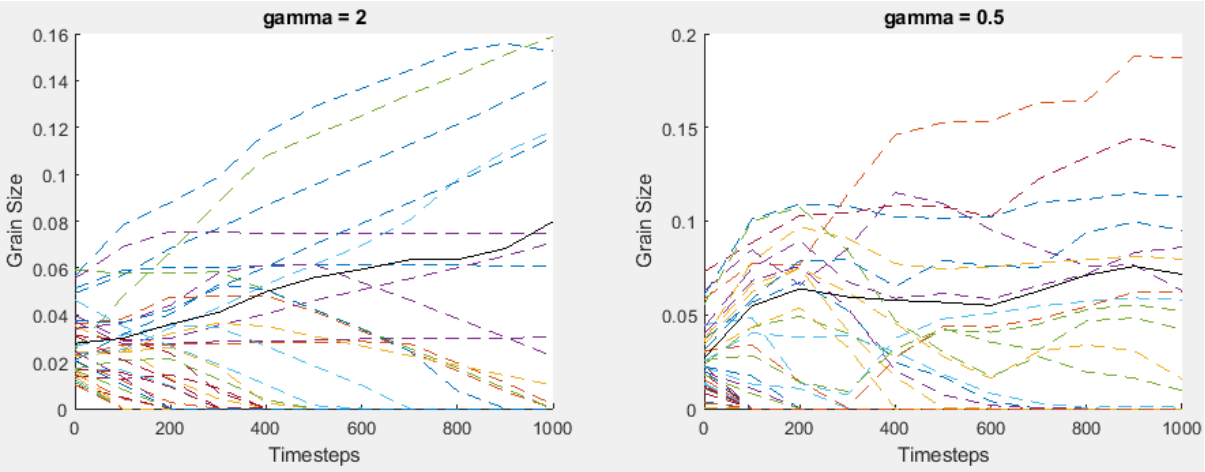

Figure 5.6: Comparison of γ-values. Plotted are the size of each grain with dotted lines, and the average grain size with a solid line. The left shows a value of 2, with even growth, while the right shows uneven erratic growth for a value of 0.5.

Both from Figures 4.12 and 4.11, it is evident that γ has very different effect on the evolution than γ and L. $\gamma = 0.5$ results in both the growth curves being erratic, as well as a significant drop in mean growth rate. Interestingly, $\gamma = 2$ also sticks out, as can be seen in Figure 4.12, dropping significantly relative to both the previous and subsequent values of the parameter.

In the evolution equation, Equation 4.2, γ is a factor for the only summation, which can illuminate the dramatic effect it has on the grain growth. For low values, the term withγ in front might be less positive than the α-term is positive, which might explain the erratic behavior.

In order to compare these parameters and growth rates directly,they have been put into Table 5.1.

5.2 Comparison with Finite Difference

As stated, the programme in this thesis utilizes a Spectral Method for modelling the evolution. The project prior to this used the Finite Difference Method, and it is interesting to compare the results of these two projects. Figure 5.7 directly compares the mean growth curves of the three different grain orientation numbers. While the curves obviously have different starting conditions, there is no obvious difference in inclination visible.

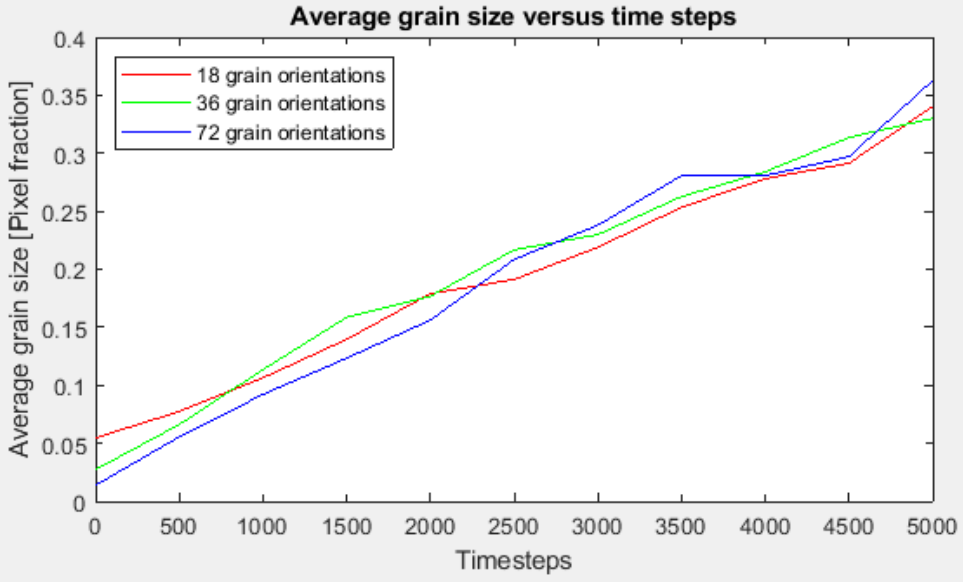

Figure 5.7: Spectral Fourier method. Plot of three different grain orientation variants, grain size with timesteps.

As mentioned in the method section, the spectral modelling uses a coarser time discretization, $dt = 1$, than the finite difference scheme, which uses $dt = 0.1$. This results in Figure 5.8, where the finite difference plot goes to 10000 steps, while the spectral plot goes to 1000. Even so, the spectral method seems to be about twice as fast, even while divided by ten. Aside from that, the plots are quite similar.

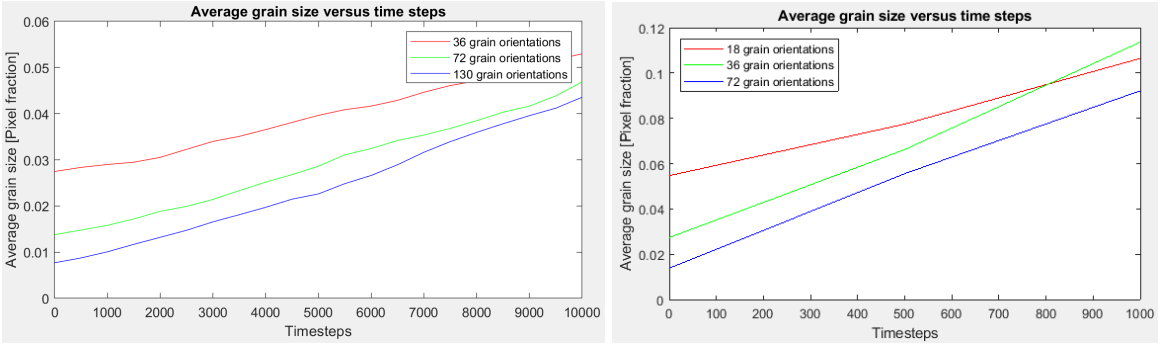

(a) Finite Difference Method

(b) Spectral Fourier Method

Figure 5.8: Plot of three different grain orientation variants, grain size with timesteps.

.

Figure 5.9 plot the same data as 5.7, but the initial grain size has been subtracted from the data, in accordance with equation 2.8. What can bee seen here is how a smaller amount of grain orientations affect the inclination of the grain growth curve, and the accuracy of the model. The curve for 18 grain orientations clearly has a lower growth than the others. The 72 grain orientation curve also shows some drop off as the grains grow and therefore also the total amount of grains orientations in the system declines.

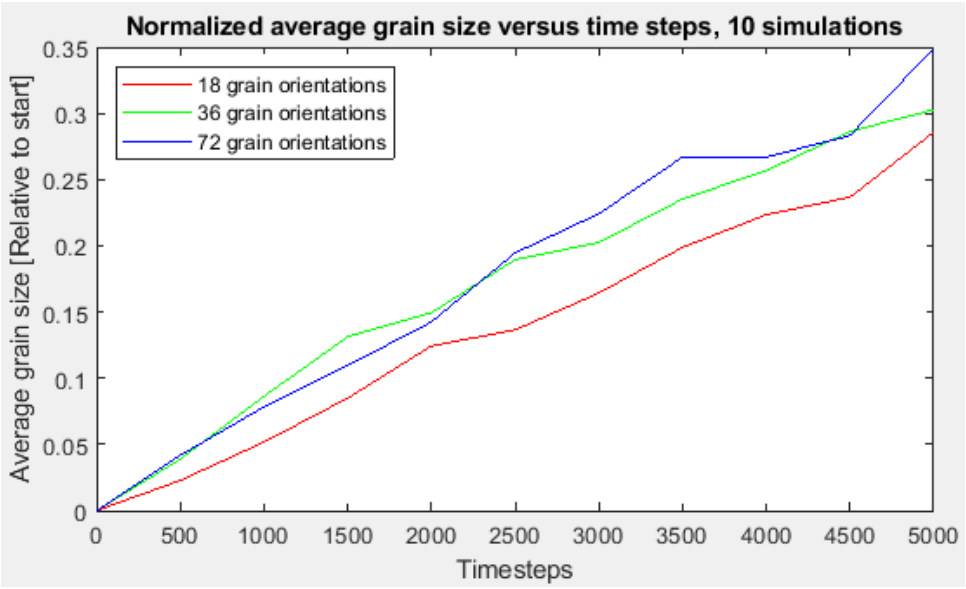

Figure 5.9: Spectral Fourier method. Plot of three different grain orientation variants, grain size with timesteps. The initial mean grain size has bean subtracted from the whole of each curve.

From Figure 5.10, it seems quite evident that the 18 grain curve is less inclined than the rest. An explaination for this, as has been touched upon before, might be that in a finite system, the

effect of the grain boundaries themselves. With fewer grains, the system approaches a stable state, and in a way, a system with fewer grains lies in the future relative to a sytem with more.

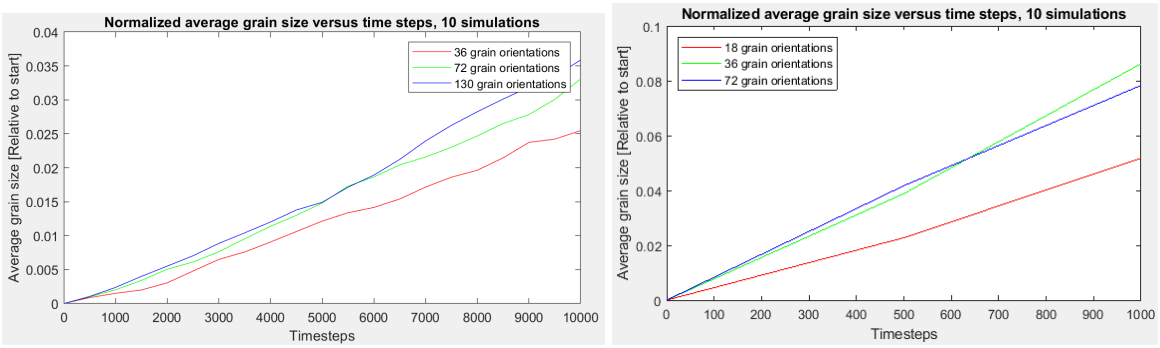

(a) Finite Difference Method **(b)** Spectral Fourier Method

Figure 5.10: Evolution of grain sizes for a single structure. Dotted lines are individual grains/field variables, and the solid line is the mean grain size.

.

Self-similarity

Considering the phenomena of self-similarity discussed on page 3 and illustrated in figure 2.2, grain distribution plots were created. The first, figure 5.12, shows the grain size distribution plot for a structure with 36 grains evolved with the spectral method. This shows a quite even lowering and displacement of the distributions with time. It can be argued that the earliest instance has a sharper peak, and that the distribution evens out as the structure develops. This is likely due to the initial structure being a bit too evenly distributed, resulting in an unnatural number of grains with a size close to the mean.

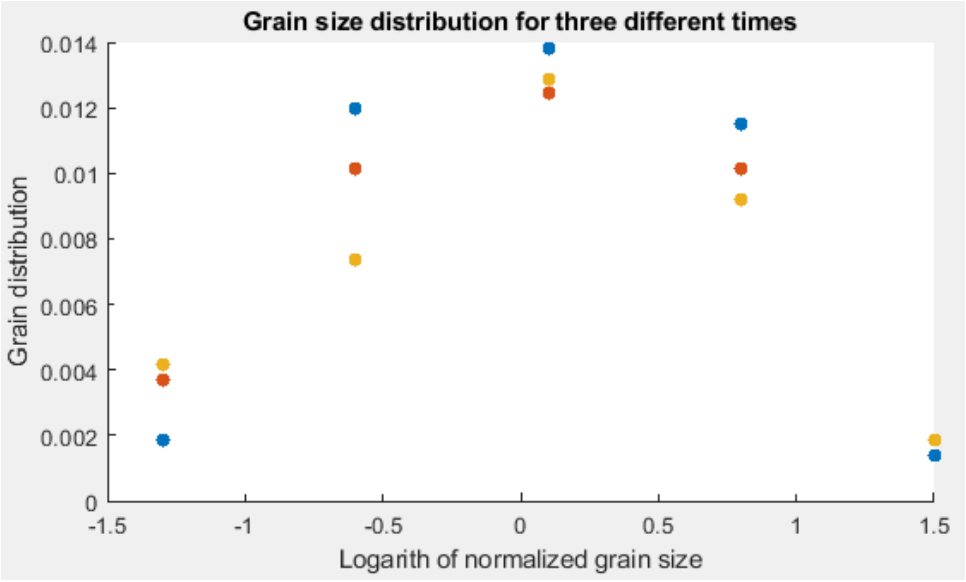

Figure 5.11: Grain size distribution plot, comparing three different points in the simulation. Illustrates the self similar nature of the grain structure over time, compare with figure 2.2.

Figure 5.12 shows the same grain distribution plot for 130 grains modelled with the finite difference method. While the principle of self-similarity itself is apparent in both plots, it is evident that the distributions them self are of different natures. One reason for this could be the number of grains. As the number of grains diminishes, the statistical accuracy of the distribution is undermined.

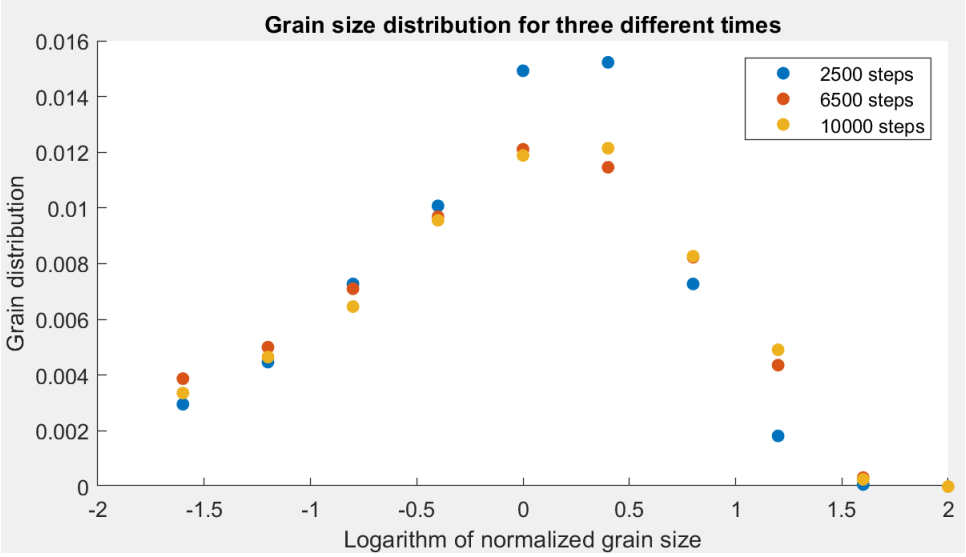

Figure 5.12: Grain size distribution plot, comparing three different points in the simulation. Illustrates the self similar nature of the grain structure over time, compare with figure 2.2.

.

6 Conclusion

The implementation of a phase-field based grain growth model has been achieved, and the results show promise. The smooth boundaries are closer to reality than sharp edges, and there is no tracking of the boundaries. Voronoi Tesselation provides a sensible starting structure for the simulations, with realistically dispersed grains. Periodic border conditions removes inaccuracies stemming from edge effects, and

The resulting grain size evolution shows linearity. Self-similarity can also be shown, and the graphical depiction of the structure itself seems to be quite realistic. The data showed some irregularity, especially with few grain orientations. This can be remedied with more grains or more parallels.

Finally a Spectral Fourier method for computing the change of the field variables and the evolution of the grain structure. This allows a much coarser time discretization, and modelling larger time intervals faster. This, in turn, helps saving computer resources and increasing computation speed.

Further work on the model should be focused on effectivizing and limiting processing time, possibly utilizing parallel processing to a more effective degree. Aside from that, more data, like free energy levels, and specific grain boundary profiles should be extracted from the structure during the process. With the phase field model, adding another phenomenon like Zener pinning should be explored.

References

[1] L. Q. Chen and W. Yang. "Computer simulation of the domain dynamics of a quenched system with a large number of nonconserved order parameters: The grain-growth kinetics". In: *Physical Review B* (Dec. 1994).

[2] L.Q. Chen. "A novel computer simulation for modeling grain growth". English. In: *Scripta Metallurgica et Materialia* 32.1 (1995). ISSN: 0956-716X.

[3] Yoshihiro Suwa and Yoshiyuki Saito. "Computer simulation of grain growth by the phase field model. Effect of interfacial energy on kinetics of grain growth". In: *Materials Transactions* 44.11 (2003), pp. 2245–2251.

[4] VL Ginzburg. "VL Ginzburg and LD Landau, J. Exptl. Theoret. Phys.(USSR) 20, 1064 (1950)". In: *J. Exptl. Theoret. Phys.(USSR)* 20 (1950), p. 1064.

[5] John W Cahn and John E Hilliard. "Free energy of a nonuniform system. I. Interfacial free energy". In: *The Journal of chemical physics* 28.2 (1958), pp. 258–267.

[6] David A. Porter, Kenneth E. Easterling, and Mohammed Y. Sherif. *Phase Transformations in Metals and Alloys*. CRC Press, Taylor and Francis Group, 2008.

[7] Frederick John Humphreys and Max Hatherly. *Recrystallization and related annealing phenomena*. Elsevier, 2012. Chap. 11, pp. 333–378.

[8] S. D. Coughlan and M. A. Fortes. "Self similar size distributions in particle coarsening". In: *Scripta metallurgica et materialia* 28.12 (1993), pp. 1471–1476.

[9] L. Q. Chen, D. N. Fan, and V. Tikare. "A Phase-Field Model for Grain Growth". In: *Metallurgical and Materials Transactions A* (July 1998).

[10] T. Keller and J. Gruber. *The Mesoscale Microstructure Simulation Project*. URL: `https://github.com/mesoscale/mmsp`.

[11] M Odegaard. "Modelling grain growth with the phase field method". Specialization Project.

[12] Matteo Frigo and Steven G Johnson. *The fastest fourier transform in the west*. Tech. rep. MASSACHUSETTS INST OF TECH CAMBRIDGE, 1997.

[13] S. Bulent Biner. *Programming Phase-Field Modeling*. Springer, 2017.

[14] Toshiyuki Koyama. "Phase field". In: *Springer Handbook of Materials Measurement Methods*. Springer, 2006, pp. 1031–1055.

[15] Samuel Miller Allen and John W Cahn. "Ground state structures in ordered binary alloys with second neighbor interactions". In: *Acta Metallurgica* 20.3 (1972), pp. 423–433.

[16] JE Burke and D Turnbull. "Recrystallization and grain growth". In: *Progress in metal physics* 3 (1952), pp. 220–292.

[17] M Hillert. “On the theory of normal and abnormal grain growth”. In: *Acta metallurgica* 13.3 (1965), pp. 227–238.

Figures

This appendix contains figures generated as part of the thesis. They are generated large, so as to be easier to read and analyse.

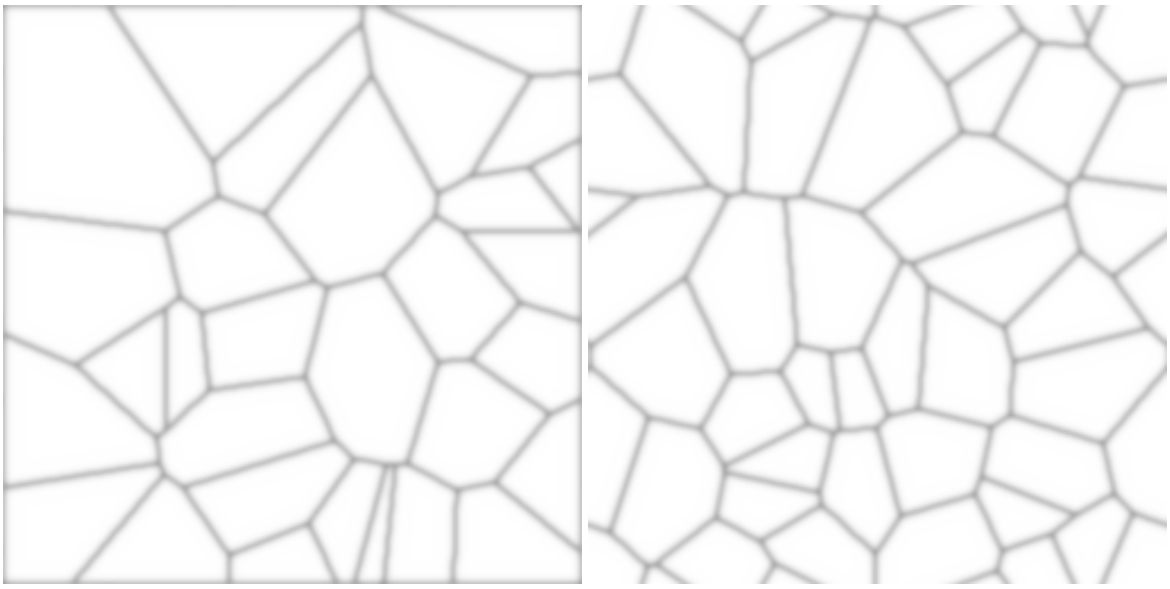

(a) Voronoi Tessellation without periodic border conditions.

(b) Voronoi Tessellation with periodic border conditions.

Figure .1: Comparison of Voronoi Tessellation with and without periodic border conditions. Other parameters are identical, but the placement of the grain seeds are random. Notice the shape of the grains close to the edges.

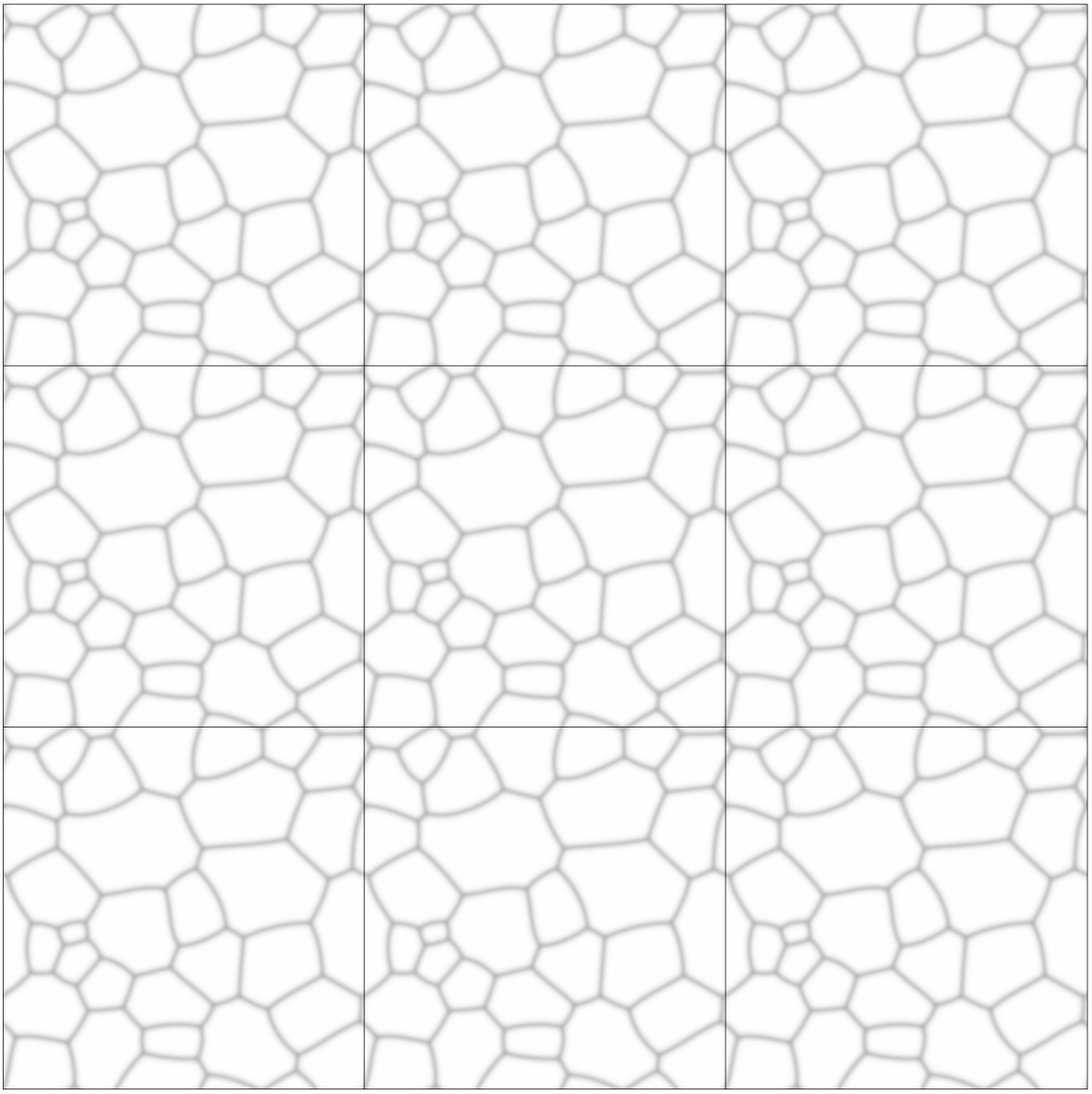

Figure .2: A three-by-three grid, repeating the initial Voronoi Tessellation.

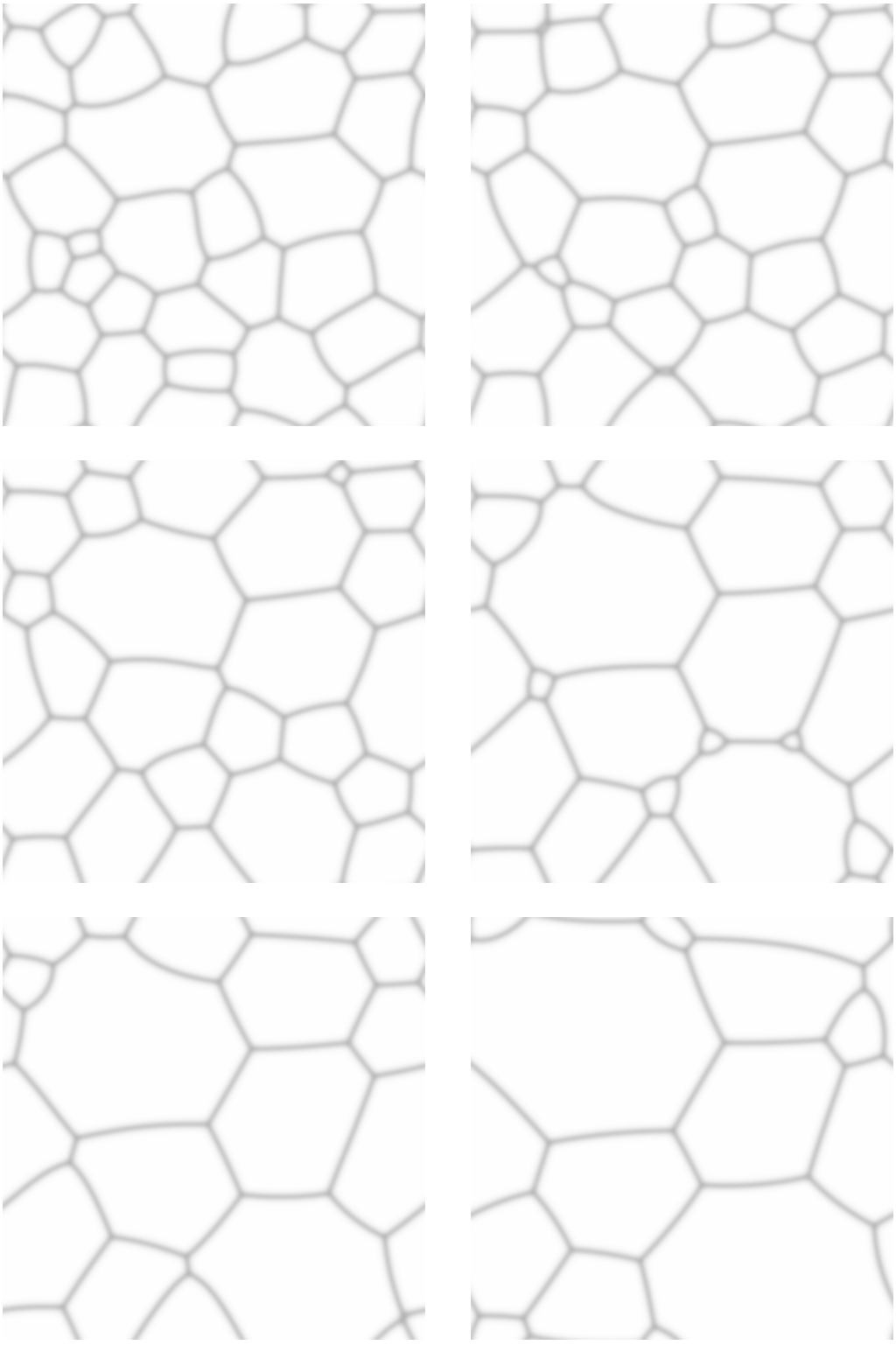

Figure .3: Visualization of the grain evolution in the model.

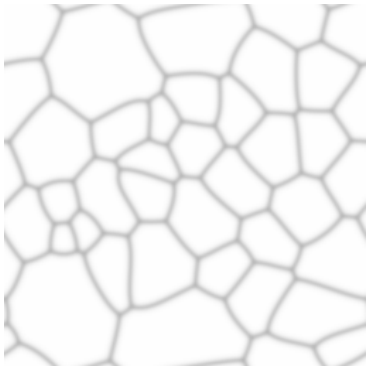

(a) 36 grains

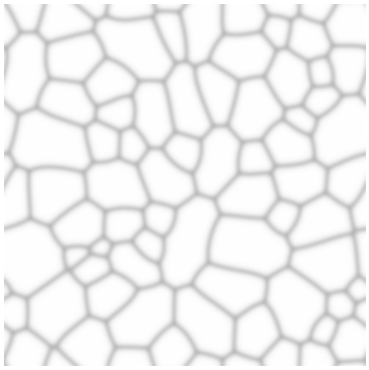

(b) 72 grains

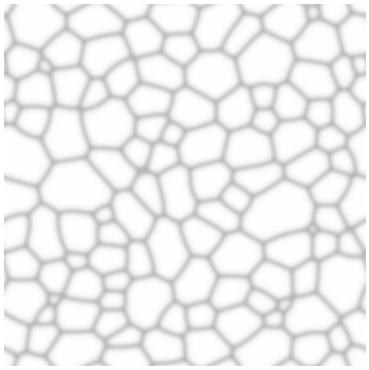

(c) 130 grains

Figure .4: Starting structure with different grain numbers/ field variables.

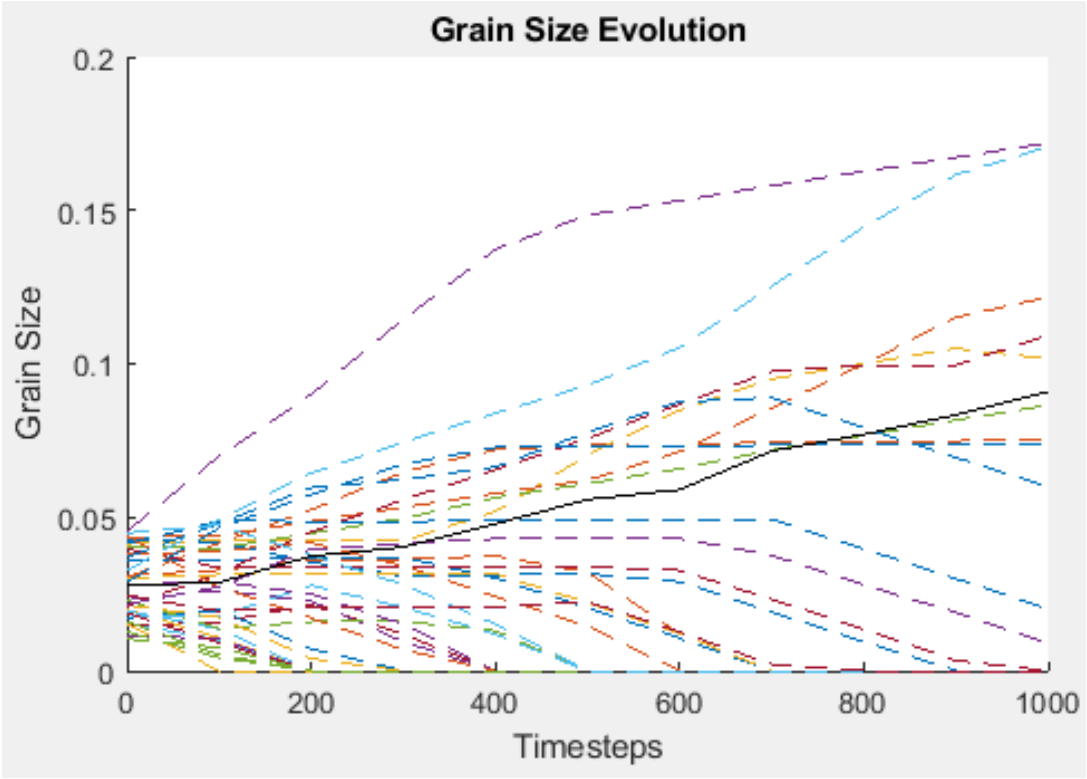

Figure .5: Evolution of grain sizes for a single structure. Dotted lines are individual grains/field variables, and the solid line is the mean grain size.

.

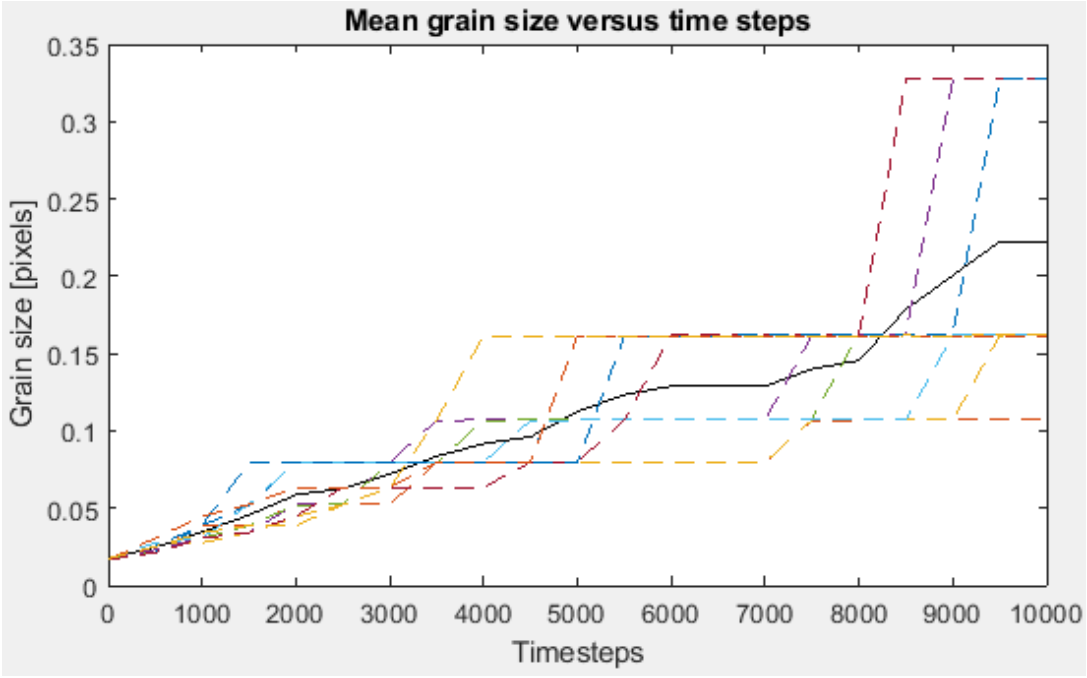

Figure .6: 18 Grains. Mean grain size evolutions of 10 different grain structures. All parameters are identical, but the initial structure is randomized. The dotted lines are individual mean grain sizes and the solid line is the mean.

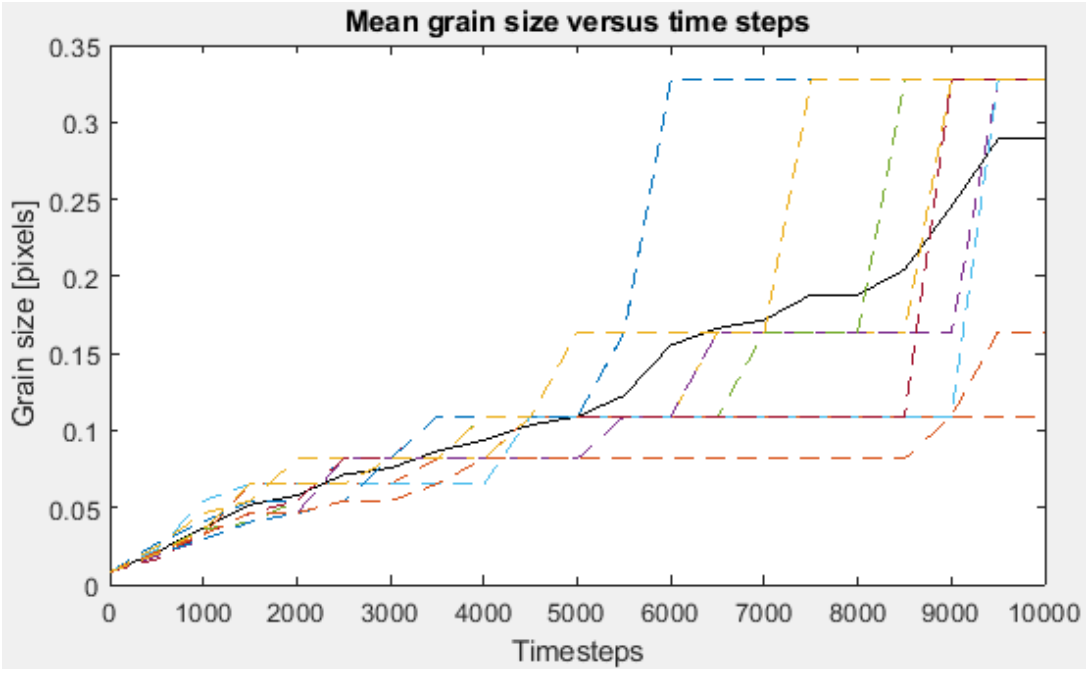

Figure .7: 36 Grains. Mean grain size evolutions of 10 different grain structures. All parameters are identical, but the initial structure is randomized. The dotted lines are individual mean grain sizes and the solid line is the mean.

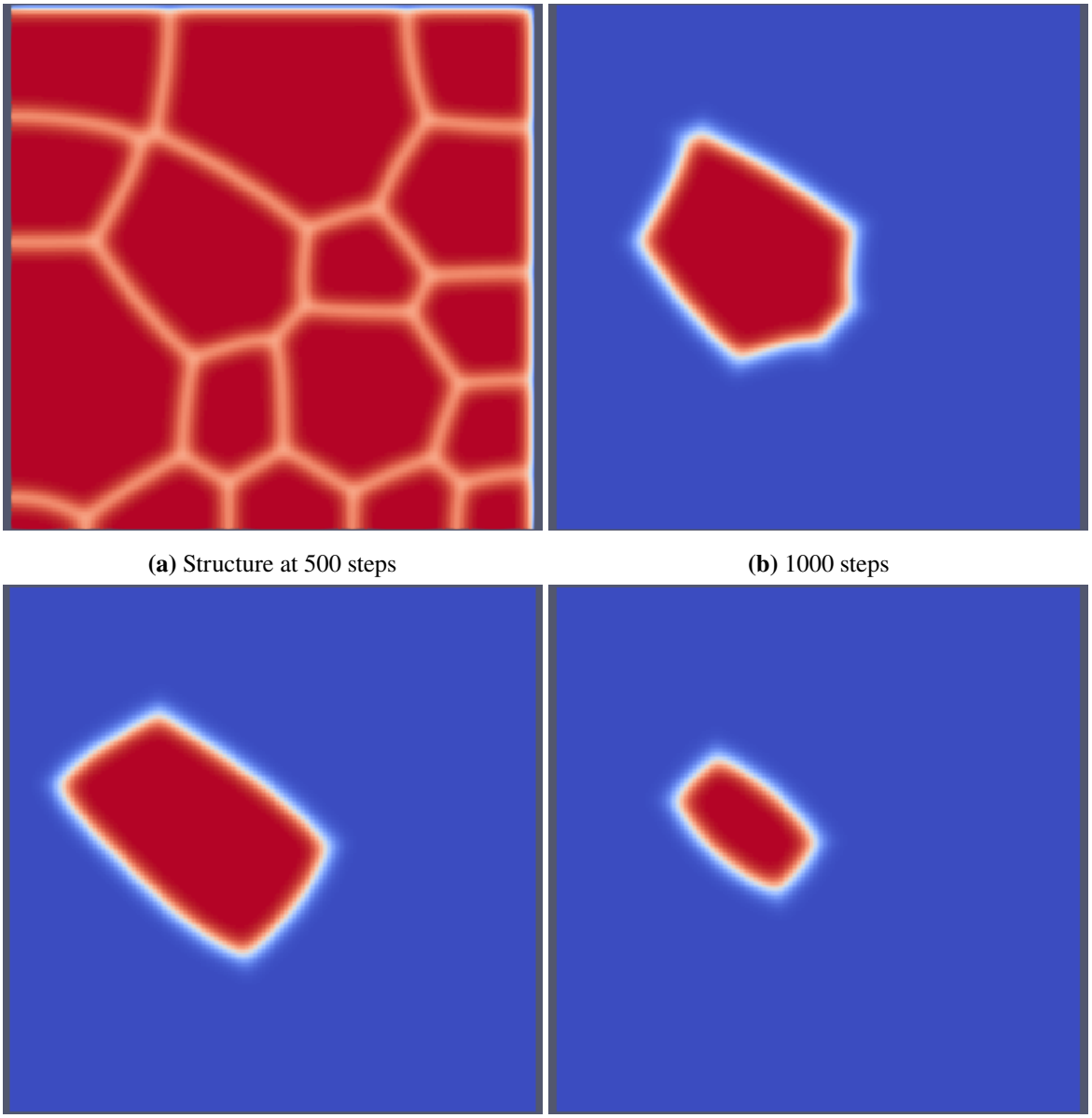

(a) Structure at 500 steps

(b) 1000 steps

(c) 1500 steps

(d) 2000 steps

Figure .8: Evolution of a single grain, as well as the initial surrounding grain structure. Spectral method, dt = 1. This also shows how the structure is analysed using software, separating the data for each grain.

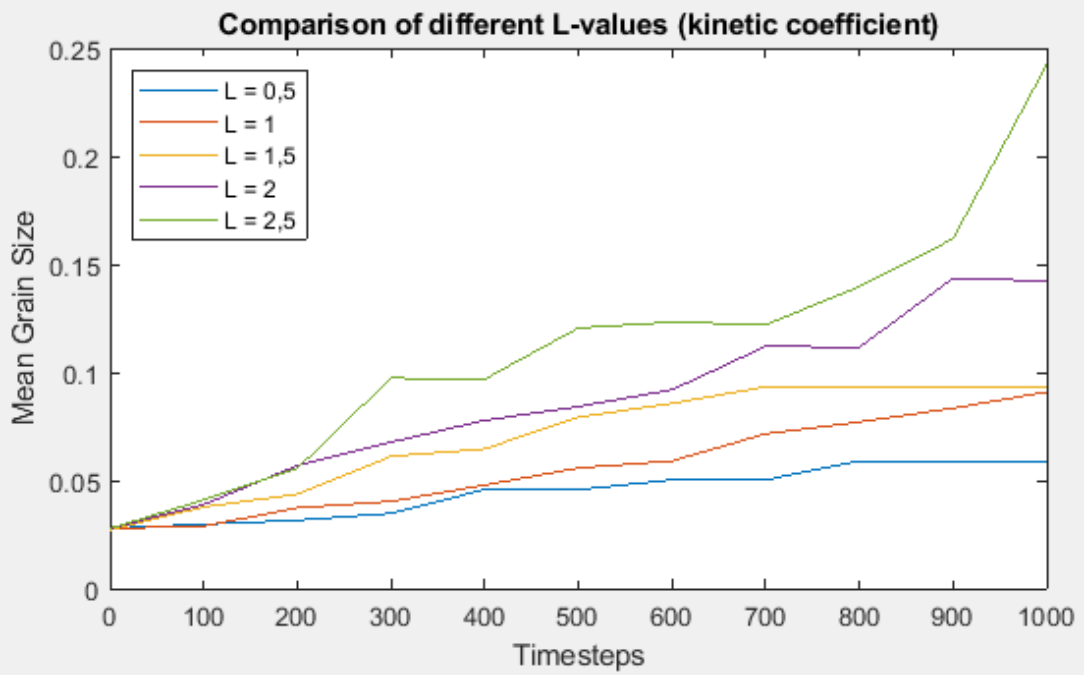

Figure .9: Average grain size plotted for five different -values.

.

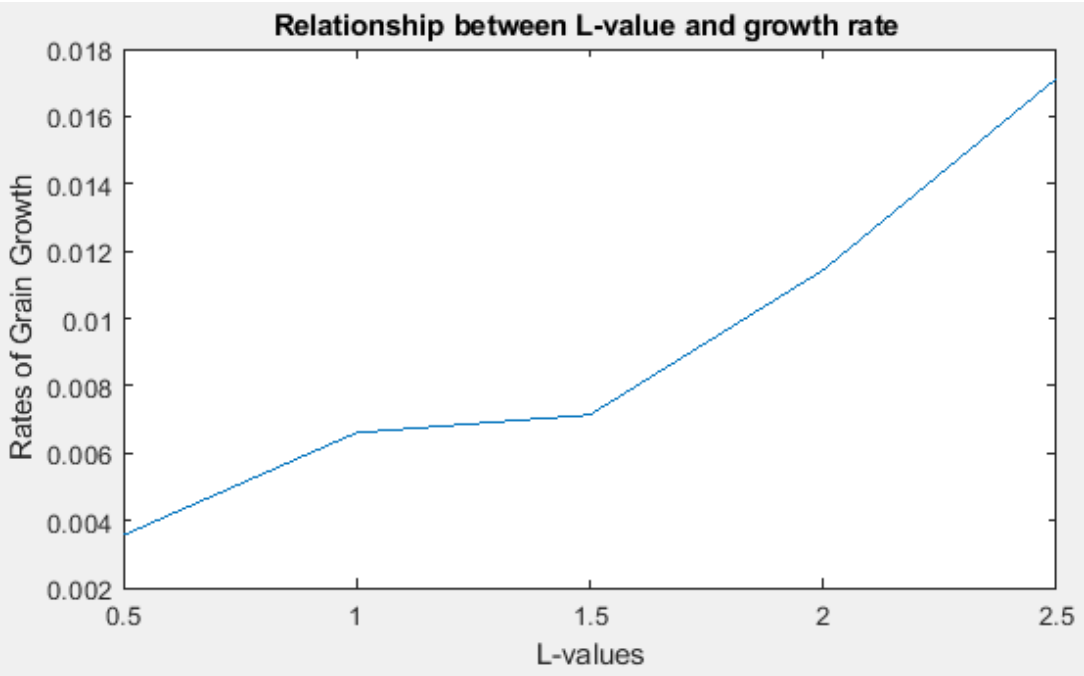

Figure .10: Grain growth plotted for increasing L-value

.

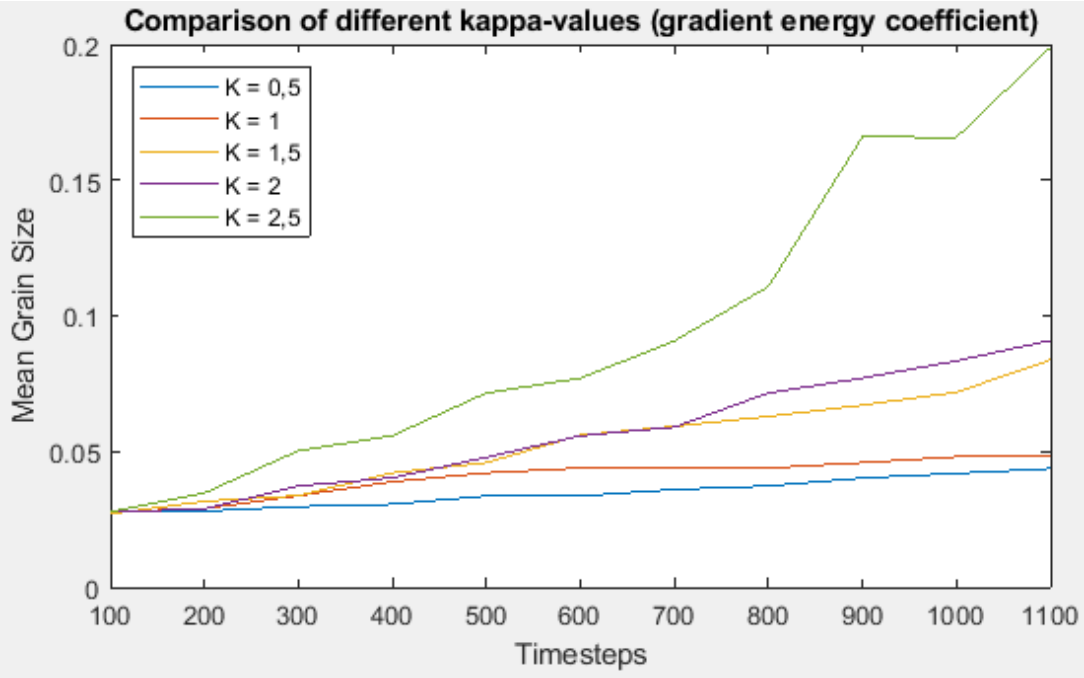

Figure .11: Average grain size plotted for five different κ-values.

.

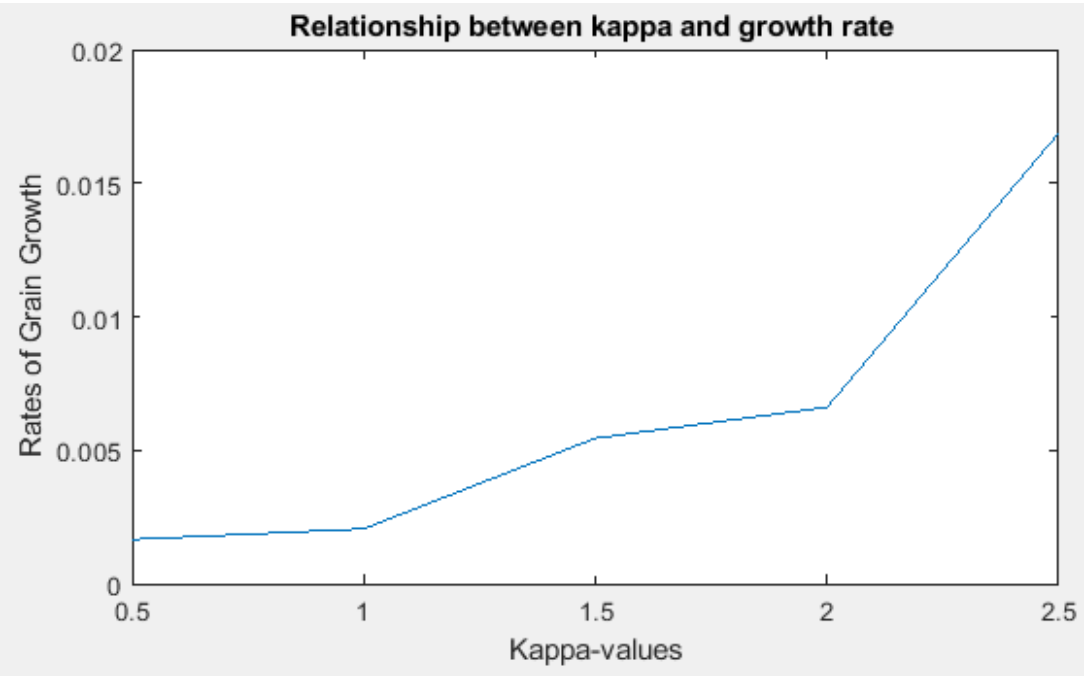

Figure .12: Grain growth plotted for increasing κ-value

.

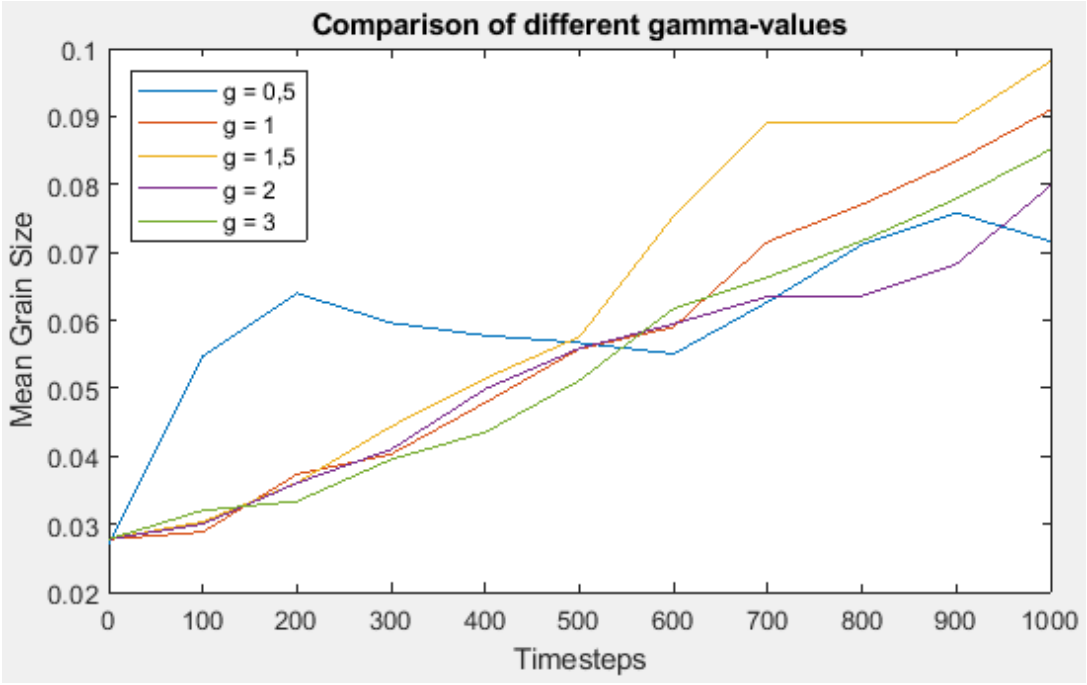

Figure .13: Average grain size plotted for five different γ-values.

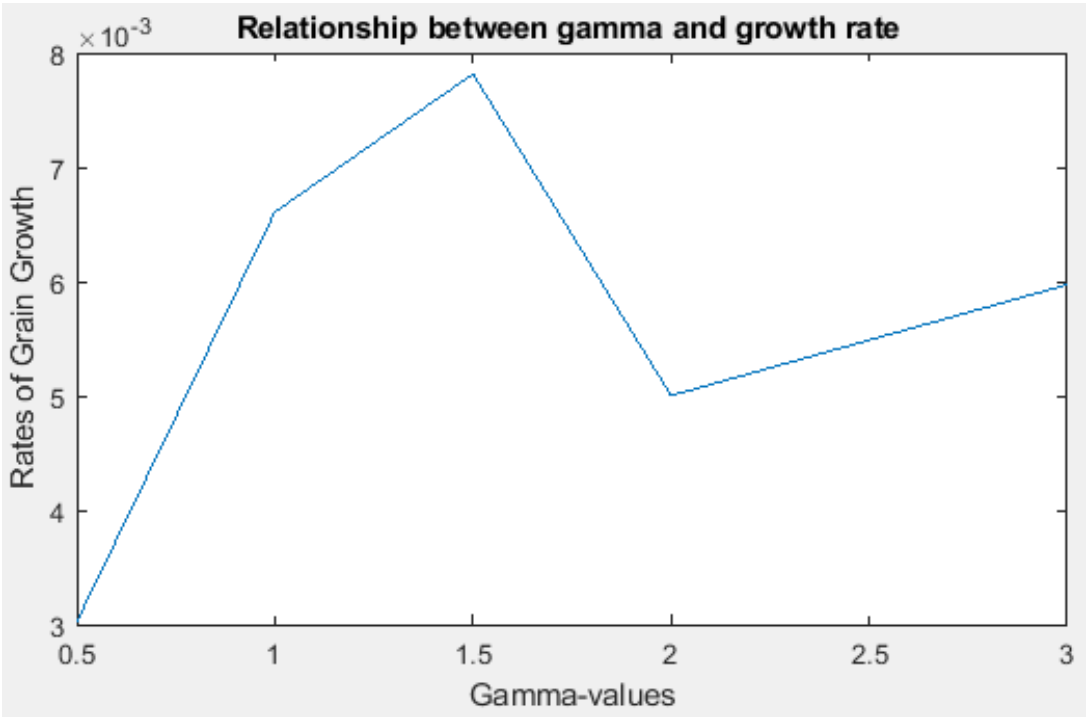

Figure .14: Grain growth plotted for increasing γ-values

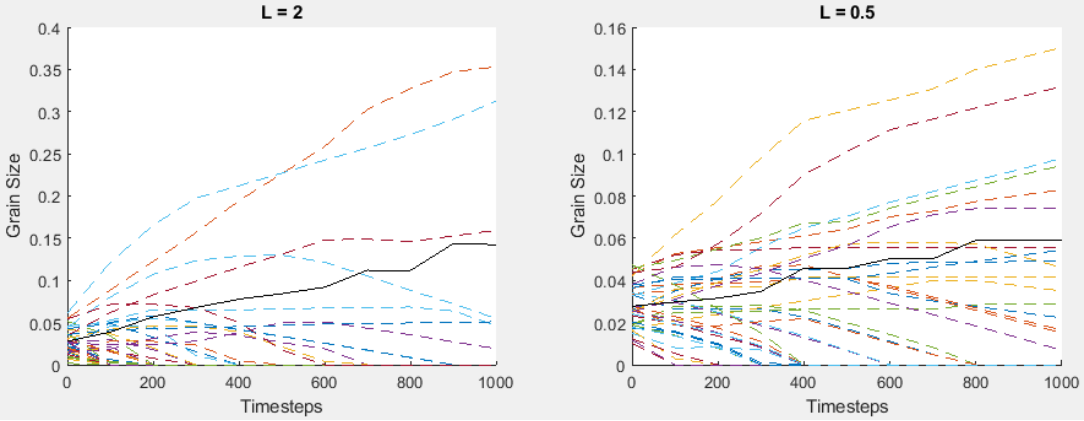

Figure .15: Comparison of L-values. Plotted are the size of each grain with dotted lines, and the average grain size with a solid line.

.

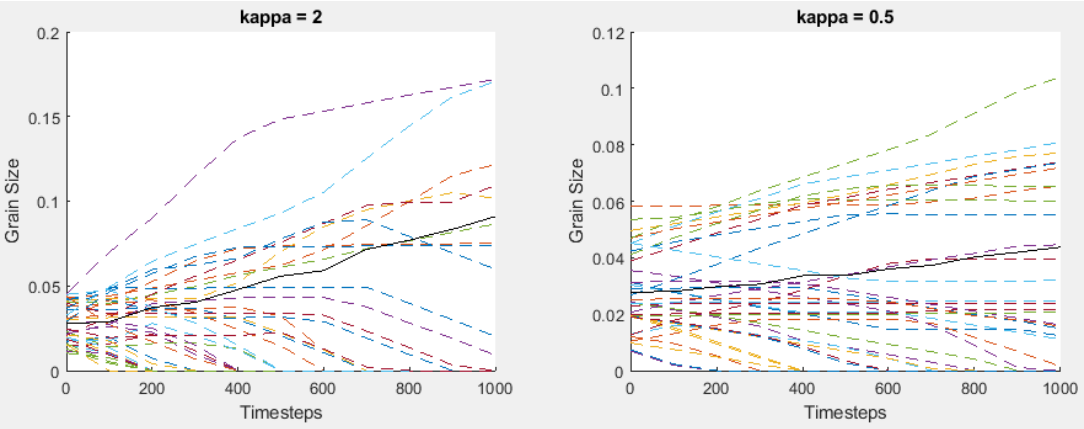

Figure .16: Comparison of κ-values. Plotted are the size of each grain with dotted lines, and the average grain size with a solid line.

.

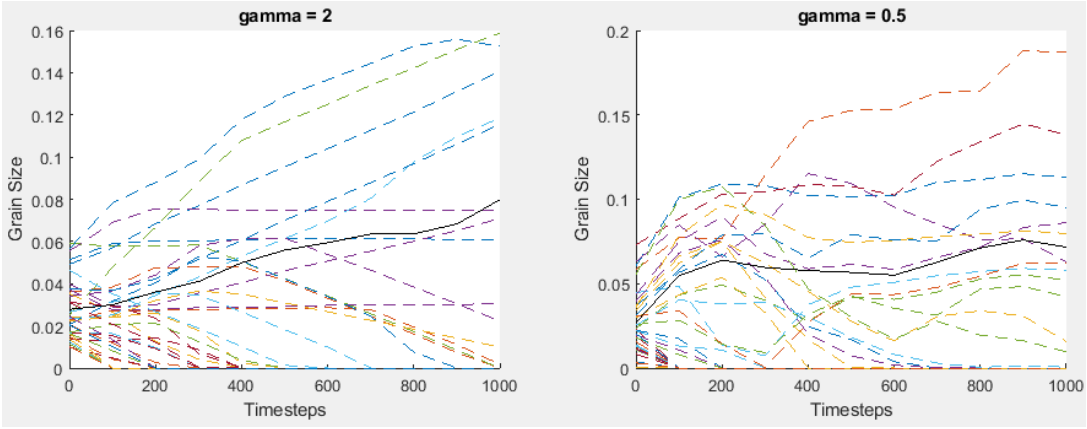

Figure .17: Comparison of γ-values. Plotted are the size of each grain with dotted lines, and the average grain size with a solid line. The left shows a value of 2, with even growth, while the right shows uneven erratic growth for a value of 0.5.

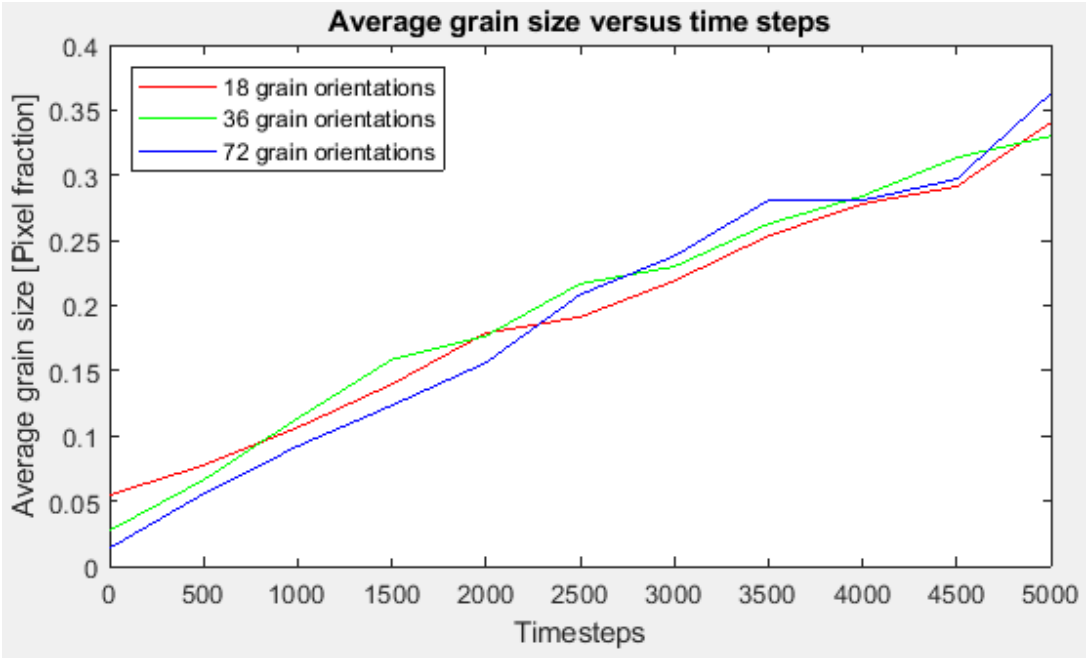

Figure .18: Plot of three different grain orientation variants, grain size with timesteps.

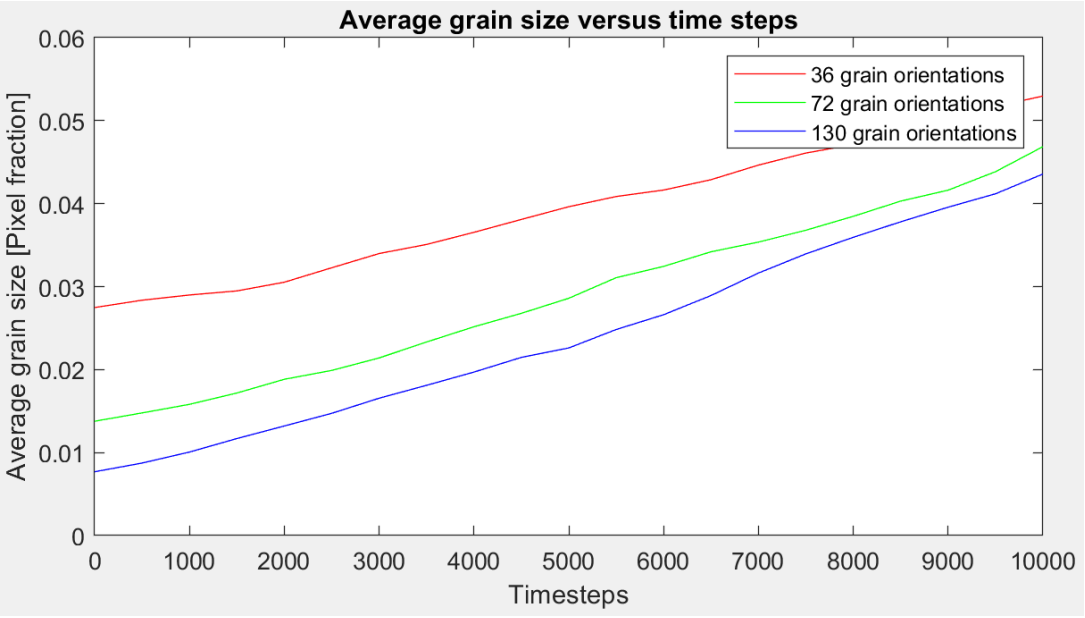

(a) Finite Difference Method

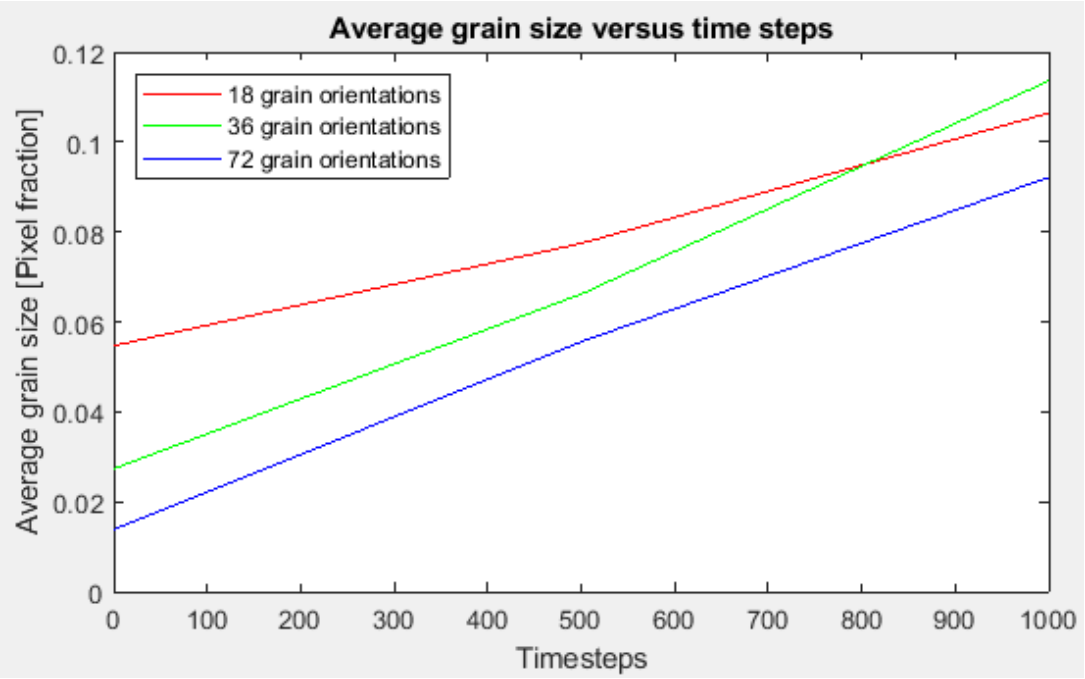

(b) Spectral Fourier Method

Figure .19: Plot of three different grain orientation variants, grain size with timesteps.

.

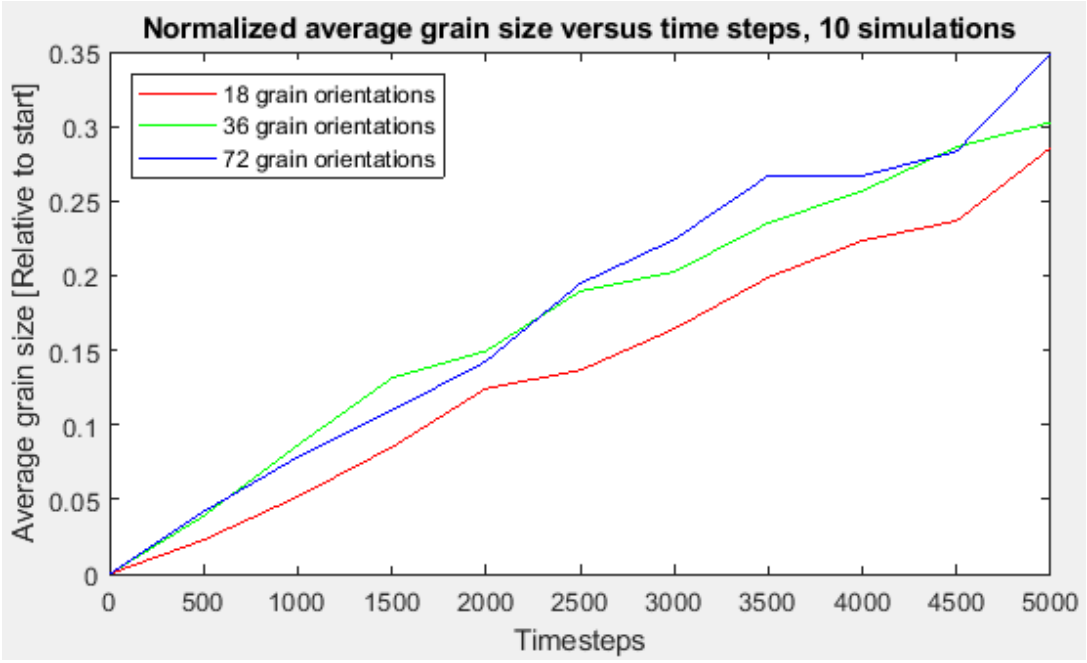

Figure .20: Plot of three different grain orientation variants, grain size with timesteps. The initial mean grain size has bean subtracted from the whole of each curve.

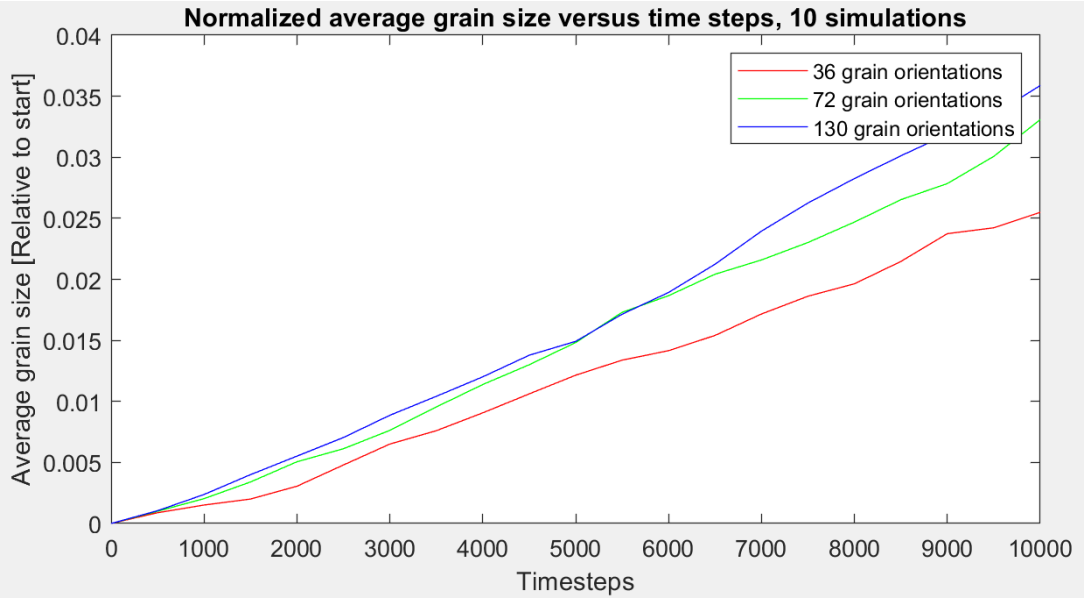

(a) Finite Difference Method

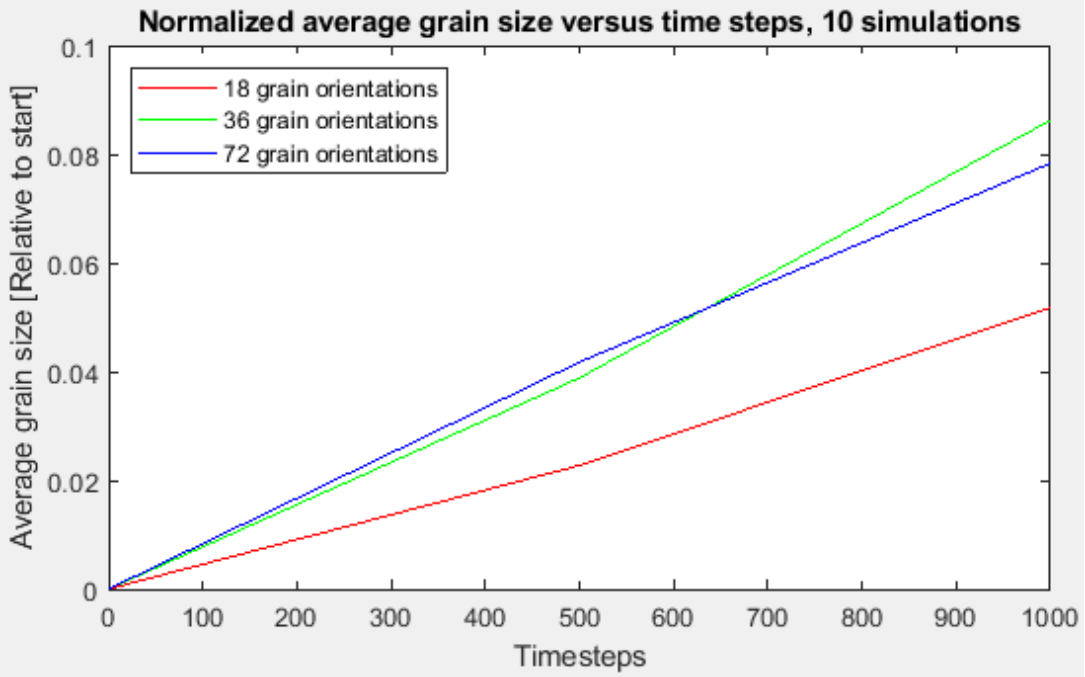

(b) Spectral Fourier Method

Figure .21: Plot of three different grain orientation variants, grain size with timesteps. The initial mean grain size has been subtracted.

.

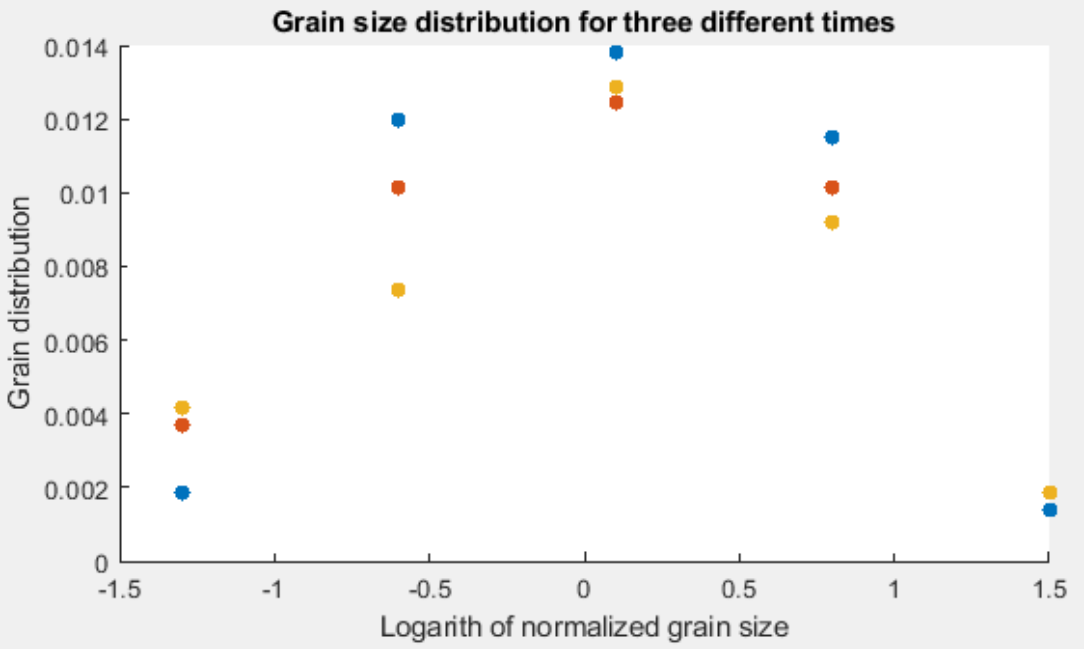

Figure .22: Grain size distribution plot, comparing three different points in the simulation. Illustrates the self similar nature of the grain structure over time, compare with figure 2.2

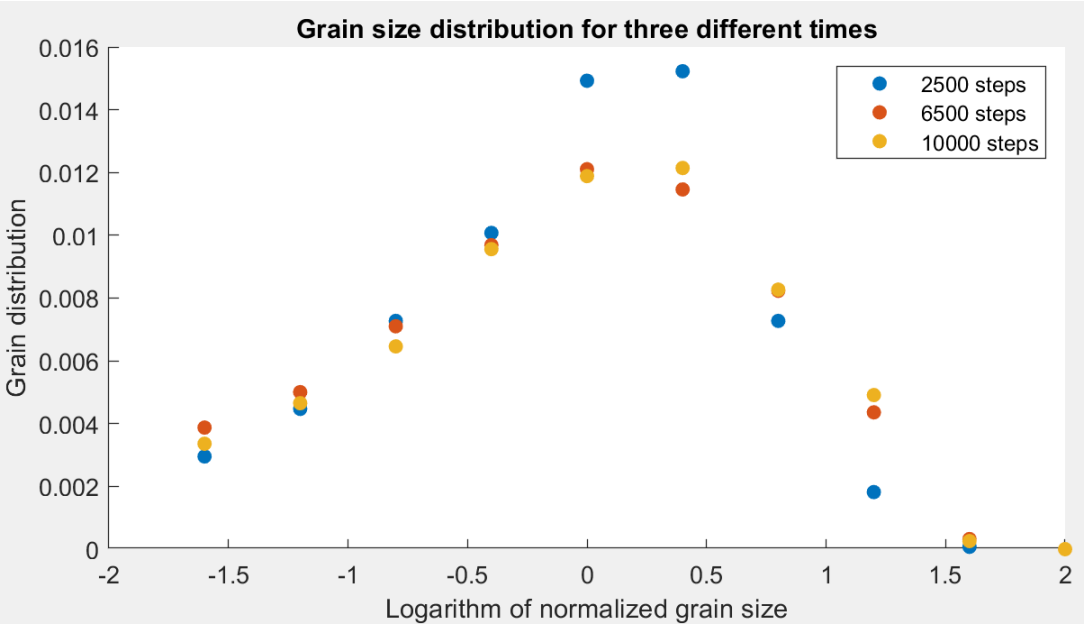

Figure .23: Grain size distribution plot, comparing three different points in the simulation. Illustrates the self similar nature of the grain structure over time, compare with figure 2.2

.

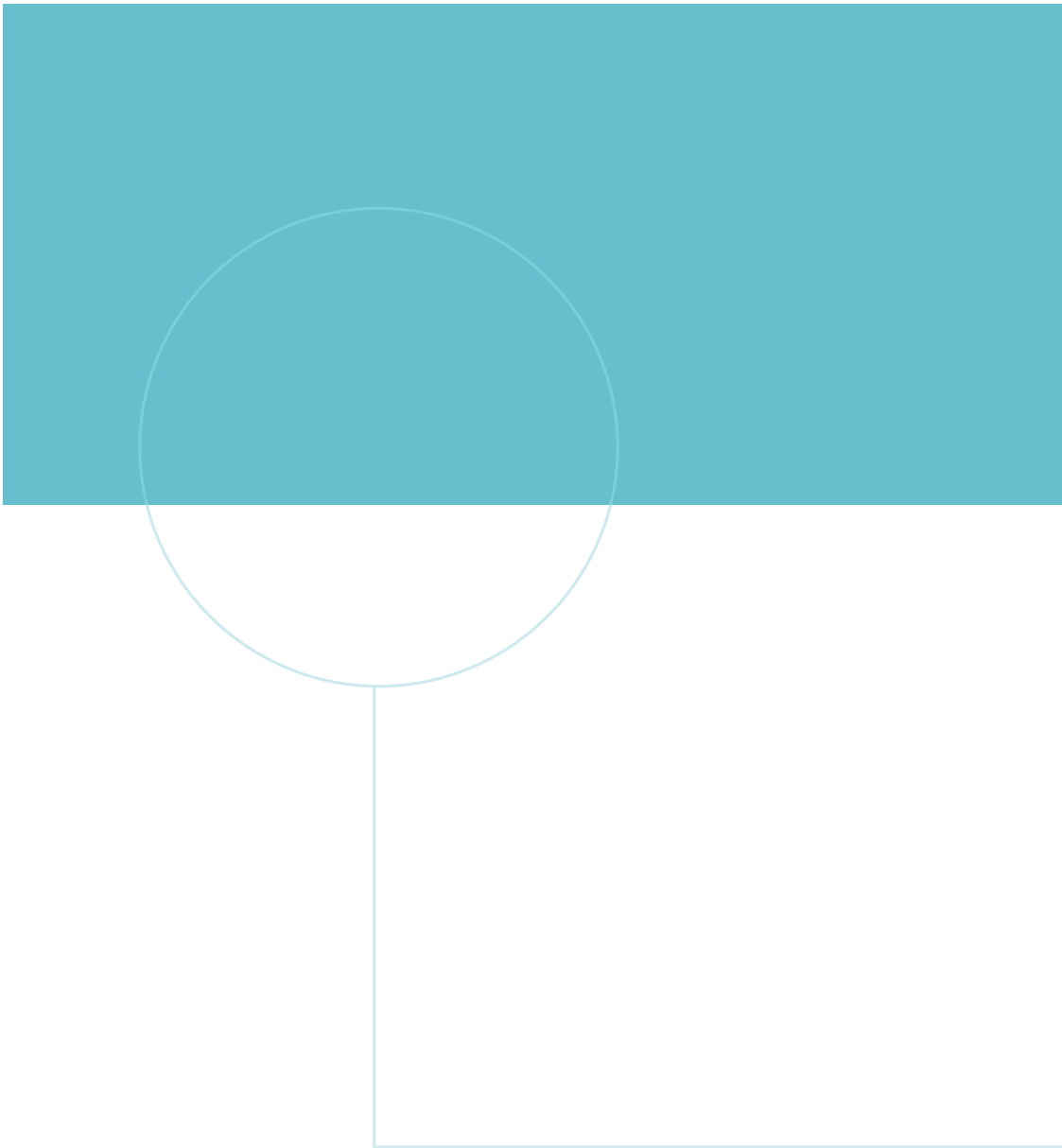

NTNU
Norwegian University of
Science and Technology